Chapter 5

Experimental results from the laboratory

In this chapter we present the experimental results of the energy spectrum, third-order structure function, absolute scaling exponents, relative scaling exponents, hierarchy transfer and probability distribution functions for turbulence produced in the wake of a cylinder in a wind tunnel. Results were obtained for an array of measuring stations at different downstream distances and for three lateral distances from the cylinder axis. These data were obtained at very high temporal resolution thus, most of the results and discussion will be dedicated to this experiment performed at the University of Warsaw by Gaudin in 1997. We also present experimental results at lower resolution of third-order structure function, absolute scaling exponents, relative scaling exponents and intermittency for jet and grid turbulence in axisymmetric water flow at different downstream distances.

5.1 Energy spectrum

The Kolmogorov relation (2.11) predicts that the energy spectrum of fully-developed homogeneous turbulence is divided into three distinct wavenumber regions: The region of energy injection at largest scales, an inertial range where the energy is transmitted from large to small scales, and a dissipative range, where the energy is dissipated by viscosity into heat from the small scales, which are compared to the Kolmogorov length scale η. In homogeneous and isotropic three-dimensional turbulence, in the inertial range, Kolmogorov (1941) proposed the $k^{-5/3}$ scaling law. Since the Kolmogorov theory K41 was published, extensive experimental and numerical studies attempted to confirm the validity of relation (2.11), in the context of three-dimensional homogeneous turbulence, Grant *et al.* (1962), Champagne *et*

al. (1970) and Frisch (1995). All these studies assumed that the power law -5/3 is observed in fully developed turbulence. The observed deviation in the $k^{-5/3}$ scaling law was invariably attributed to departures from the homogeneous and stationary conditions of the flow.

In contrast, in non-homogeneous turbulence, the universality of the power spectrum seems to be absent. Babiano (2000) demonstrated in his numerical study for 2D non-homogeneous turbulence, that the spectral slope increases with the degree of non-homogeneity and can reach up to k^{-3}. This anomalous scaling is also confirmed by our experimental results concerning the 3D energy cascade.

The energy spectrum was computed using the Fast Fourier Transform (FFT). The length of an observational data run is normally split into short sections for numerical processing. The optimum section length is the shortest that still gives reliable estimates for the spectral levels. Using a section length as short as possible but covering all relevant dynamical scales leads to better data with less noise. For the present analysis, the data were processed using a section length of N=2048 points.

Figures 5.1, 5.2 and 5.3 show the energy spectra compensated for Kolmogorov's scaling $k^{5/3}$ as a function of the non-dimensional wavenumber $k\eta$, where η is Kolmogorov's length-scale calculated using the usual definition $\epsilon = 15\nu\langle(\frac{\partial u_i}{\partial x_i})\rangle^2$, at downstream distances $X/D = 2, 4, 7, 20$ from the cylinder in the lateral positions $Y/D = -0.8$, $Y/D = -0.4$ and $Y/D = 0$ respectively. The range of values for the dissipation and the Kolmogorov length scale were 800 $m^2s^{-3} < \epsilon <$ 3700 m^2s^{-3} and 2.7 10^{-5}m $< \eta <$ 4.5 10^{-5}m. At the points near the cylinder, some coherent structures produced by the Karman vortex street play a dominant role on the flow structure, and a strong vorticity component aligned with the cylinder axis introduces some two dimensional effects. The spikes that appear in the spectrum at low wave numbers for $X/D \leq 7$ at the three lateral distances, are due to Karman vortex shedding similar to those found by Chilla *et al.* (1996). One observes that deviations from the -5/3 law occur in all downstream distances at the three lateral distances up to $X/D = 20$. The steepness of the energy spectrum decreases with the downstream distances from the cylinder. It greater near the source of turbulence, where the flow is non-homogeneous. This non-universality in the spectral slope seems due to the coherent structures and their contribution to the transfer dynamics. The important observation is that energy spectrum is steeper than $k^{-5/3}$, which clearly indicates that the dynamics in these regions tends to be nonlocal. It could be erroneous to assign the deviation from the $k^{-5/3}$ behavior only to the intermittency phenomenon at such short distances from the cylinder. Here, two different phenomena contribute to the deviation from Kolmogorov's self-similar prediction: the nonlocal dynamics and the intermittency. Far from the cylinder, the coherent structures become less and less pronounced, the dynamics remains local and the turbulence tends to be more homogeneous.

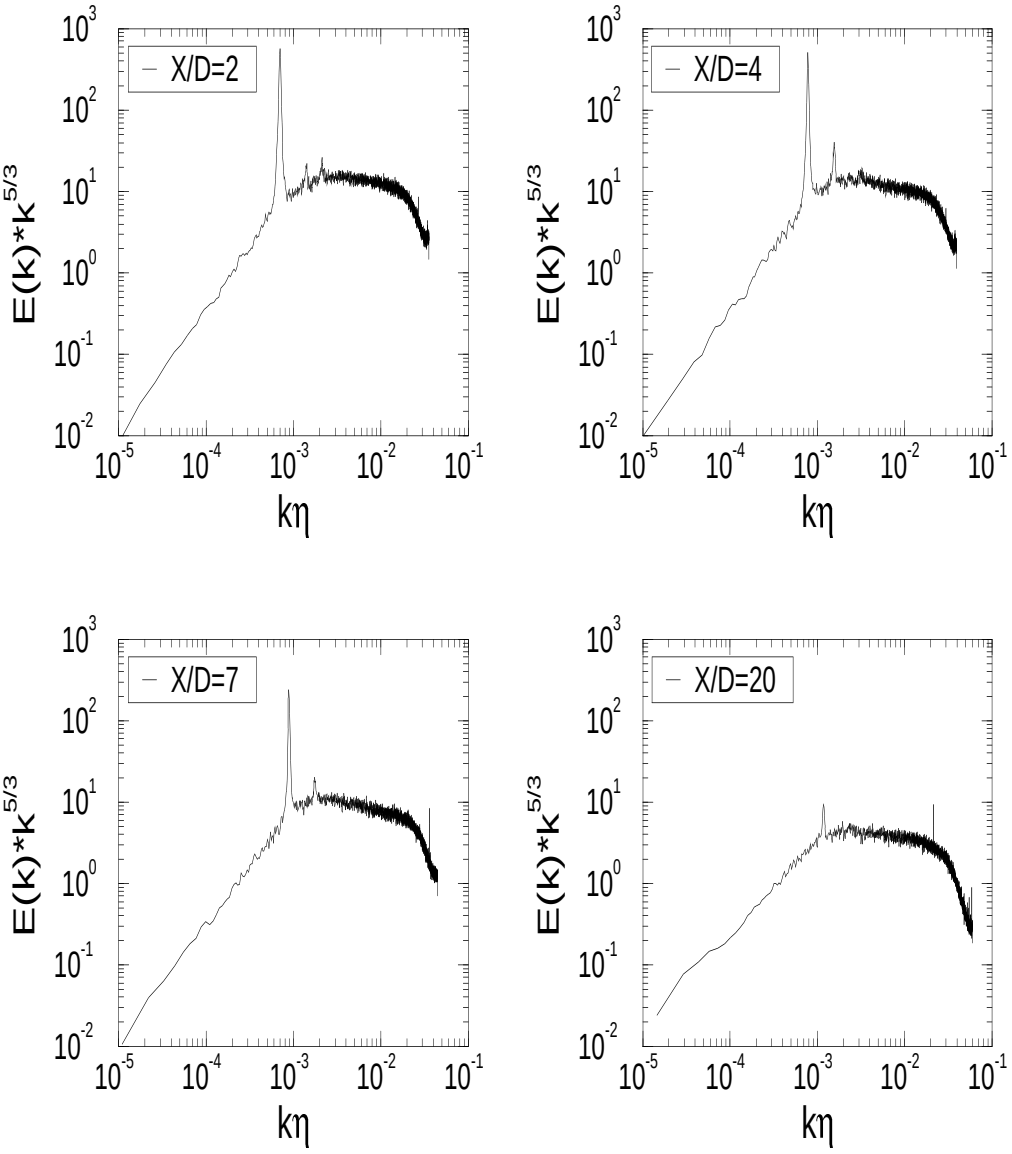

Figure 5.1: The energy compensated spectrum $E(k) * k^{5/3}$ as function of $k\eta$, for cylinder turbulence for the lateral plane $Y/D = -0.8$, at the downstream distances $X/D = 2$, $X/D = 4$, $X/D = 7$ and $X/D = 20$ respectively from the cylinder.

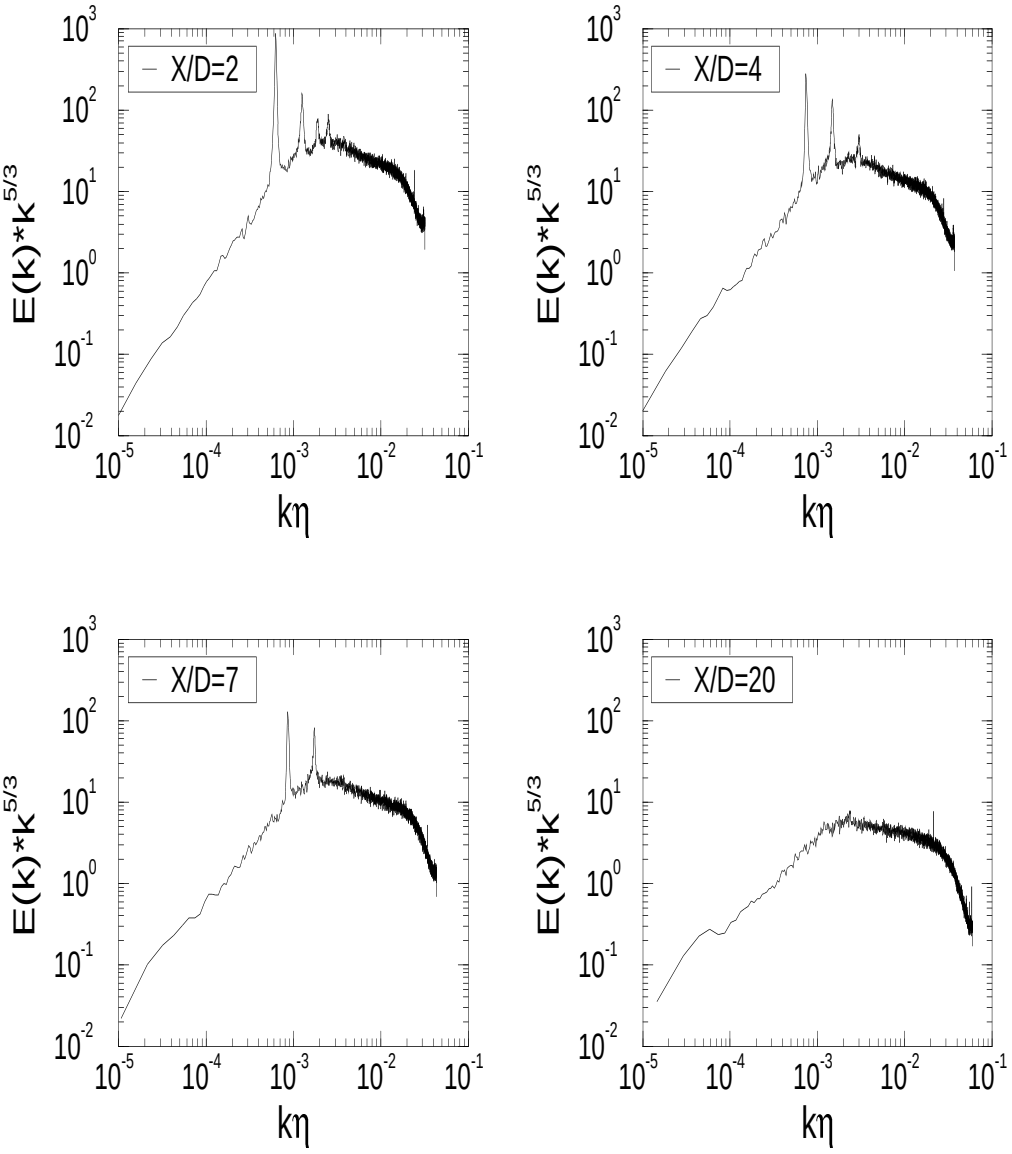

Figure 5.2: The energy spectrum $E(k)*k^{5/3}$ as function of $k\eta$, for cylinder turbulence for the lateral plane $Y/D = -0.4$, at the downstream distances $X/D = 2$, $X/D = 4$, $X/D = 7$ and $X/D = 20$ respectively from the cylinder.

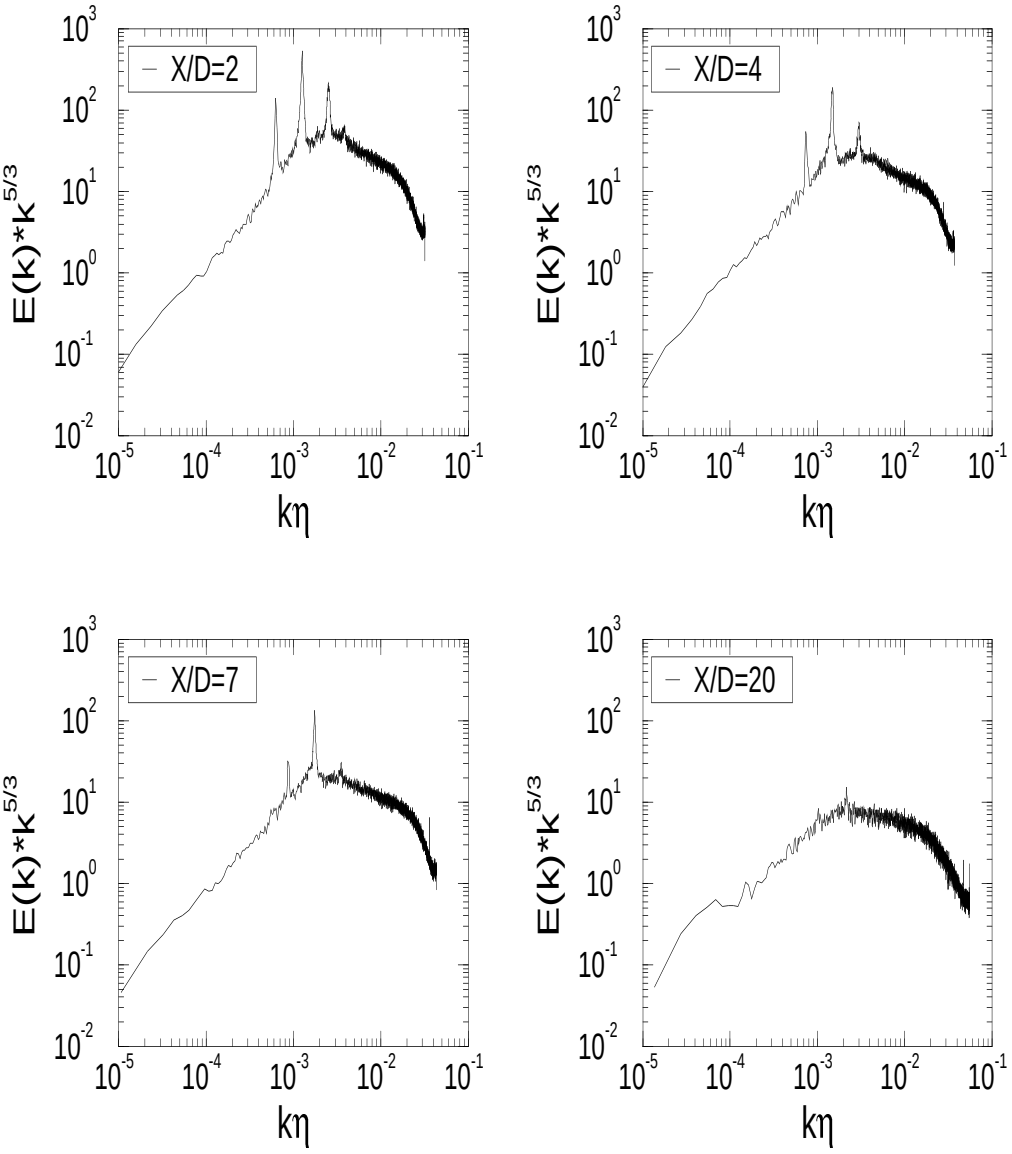

Figure 5.3: The energy spectrum $E(k)*k^{5/3}$ as function of $k\eta$, for cylinder turbulence for the lateral plane $Y/D = 0$, at the downstream distances $X/D = 2$, $X/D = 4$, $X/D = 7$ and $X/D = 20$ respectively from the cylinder.

5.2 Third-order structure function

As was mentioned before, the third-order longitudinal structure function of the velocity difference deserves special attention, because of its proportionality to the separation distance ℓ in the inertial range and it is a standard procedure in the longitudinal analysis to define an inertial range where the third-order scaling exponent ζ_3 should have the value 1 as predicted by Kolmogorov (1941).

Incidentally Benzi *et al.* (1993) used structure functions of the absolute value of the velocity increments in their investigation for homogeneous and isotropic flows; they assumed that $\mid \langle \delta u_\ell^3 \rangle \mid$ is proportional to $\langle \mid \delta u_\ell \mid^3 \rangle$. Although Boratav & Pelz (1997) found that $\mid \langle \delta u_\ell^3 \rangle \mid$ is proportional to $\langle \mid \delta u_\ell \mid^3 \rangle$, Pearson & Antonia (1997) noted that $\mid \langle \delta u_\ell^3 \rangle \mid \sim \langle \mid \delta u_\ell \mid^3 \rangle^\alpha$ with the proportionality less than 1 and α, of order 0.9, showing a weak dependence on R_λ. This proportionality is not always satisfied in homogeneous flows because it was demonstrated experimentally in jet turbulence by Herweijer *et al.* (1995) that the slope of the log-log plot of $\mid \langle \delta u_\ell^3 \rangle \mid$ versus $\langle \mid \delta u_\ell \mid^3 \rangle$ is different from unity.

In non-homogeneous and non-isotropic turbulence this proportionality is not warranted. With the aim of investigating further this issue, we compared $\langle \delta u_\ell^3 \rangle$ and $\langle \mid \delta u_\ell \mid^3 \rangle$ as a function of non-dimensional scale ℓ/η. The results are displayed in figures 5.4 to 5.6 for the three lateral positions $Y/D = -0.8$, $Y/D = -0.4$ and $Y/D = 0$ respectively, at different downstream distances X/D from the cylinder for the structure functions without using the absolute value and figures 5.7 to 5.9 show the corresponding values using the absolute value of the velocity differences. The frame *a* in figures 5.4 to 5.9 indicates data from measuring stations at $X/d = 2, 3, 4, 5, 7$ near the cylinder, less than 8 cylinder diameters away and frame *b* show the data from the more distant measuring stations at $X/D = 10, 15, 20, 40, 80$.

In figures 5.4, 5.5 and 5.6 we find that in all cases, $\langle \delta u_l^3 \rangle$ is not a simple function of the downstream distance but there is a clear distinction between the points that are near to or far from the cylinder, which show negative values. One might speculate that the observed positive and negative defined third-order structure function is the signature of complex space distribution of the energy transfers in the cylinder wake. The sign change in the third-order structure function is progressively inhibited far away from the cylinder, where the observed behavior is in agreement with a dominant average direct energy cascade scenario (negative defined $\langle \delta u_\ell^3 \rangle$).

In contrast, when the third-order structure functions are calculated by taking the absolute value (figures 5.7, 5.8 and 5.9) as is common in ESS, then a regular monotonous increasing behavior is observed in all cases. Note for example the sign-change of $\langle \delta u_l^3 \rangle$ at $X/D = 2$ and the respective data for the absolute averaged velocity differences values. The information given in figures 5.4, 5.5 and 5.6 that there are some instances of inverse cascade behavior near the cylinder is lost in figures 5.7, 5.8 and 5.9 when absolute values are used.

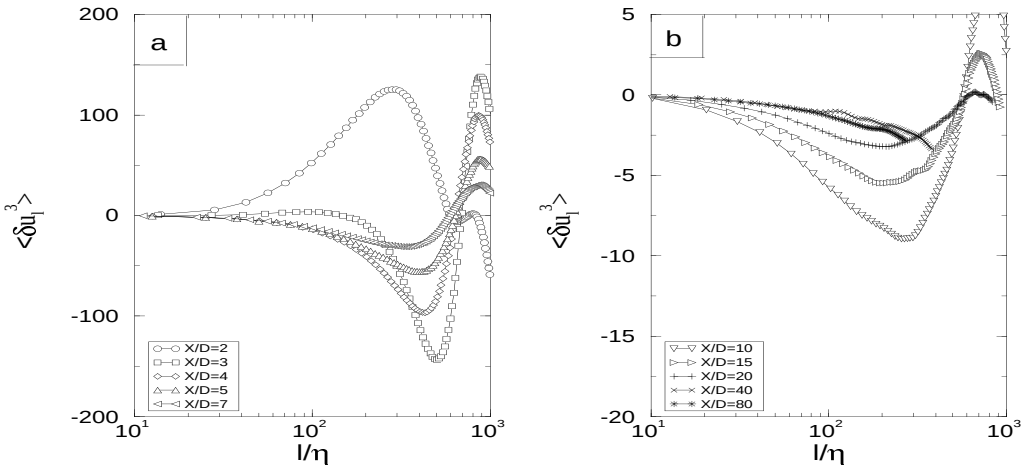

Figure 5.4: Comparison between $\langle \delta u_\ell^3 \rangle$ as a function of ℓ/η, for the lateral plane $Y/D = -0.8$, at different downstream distances X/D from the cylinder.

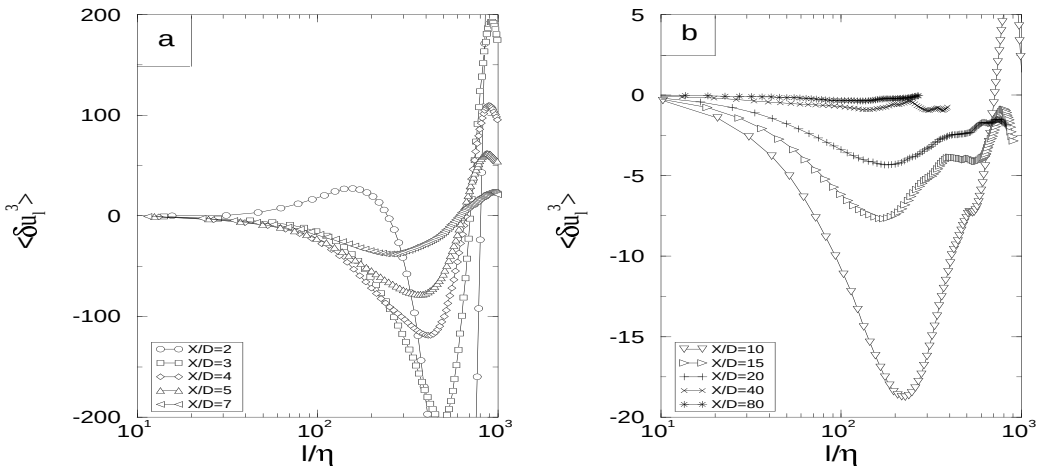

Figure 5.5: Comparison between $\langle \delta u_\ell^3 \rangle$ as a function of ℓ/η, for the lateral plane $Y/D = -0.4$, at different downstream distances X/D from the cylinder.

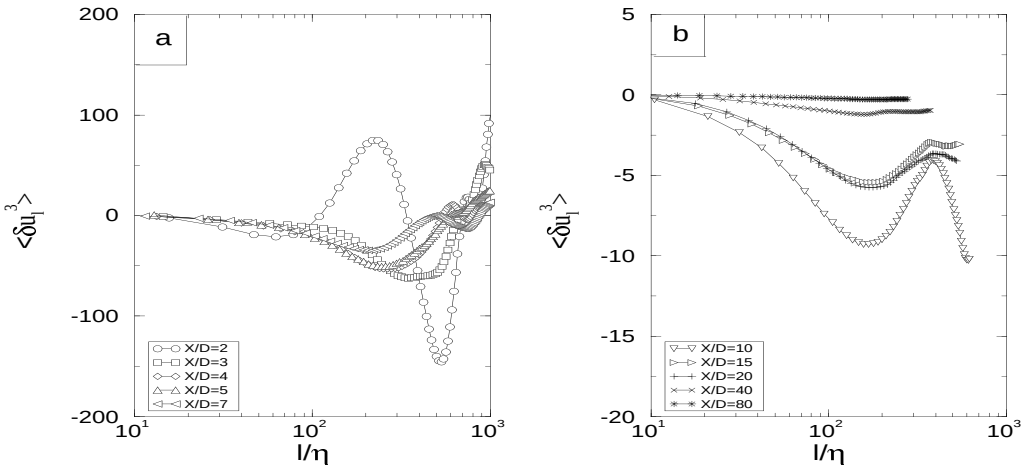

Figure 5.6: Comparison between $\langle \delta u_\ell^3 \rangle$ as a function of ℓ/η, for the lateral plane $Y/D = 0$, at different downstream distances X/D from the cylinder.

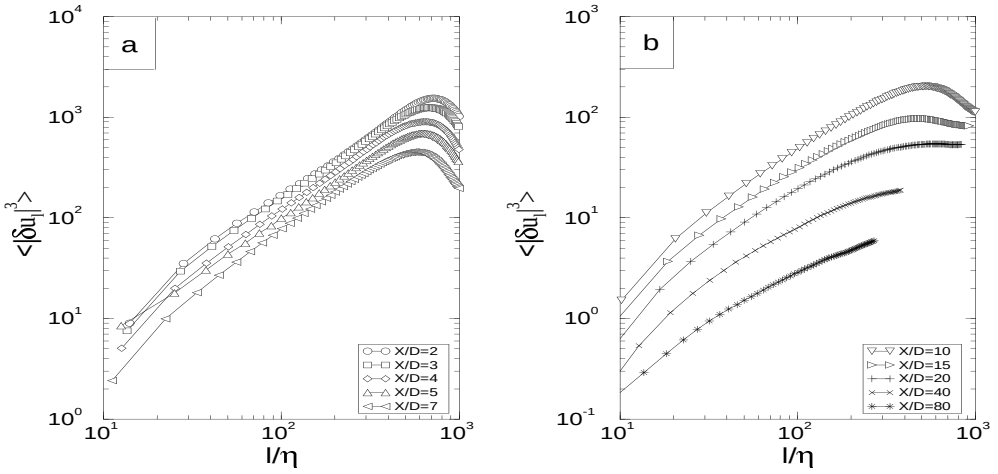

Figure 5.7: Comparison between $\langle \mid \delta u_\ell \mid^3 \rangle$ as a function of ℓ/η, for the lateral plane $Y/D = -0.8$, at different downstream distances X/D from the cylinder.

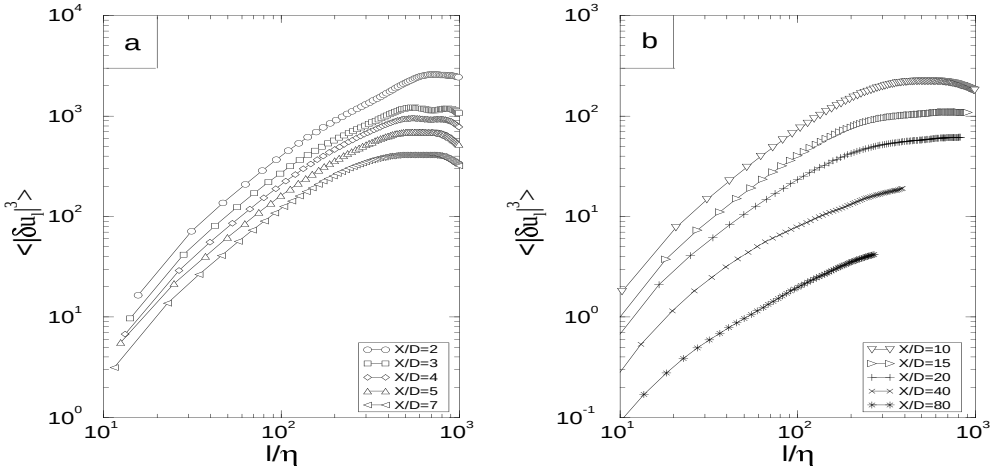

Figure 5.8: Comparison between $\langle \mid \delta u_\ell \mid^3 \rangle$ as a function of ℓ/η, for the lateral plane $Y/D = -0.4$, at different downstream distances X/D from the cylinder.

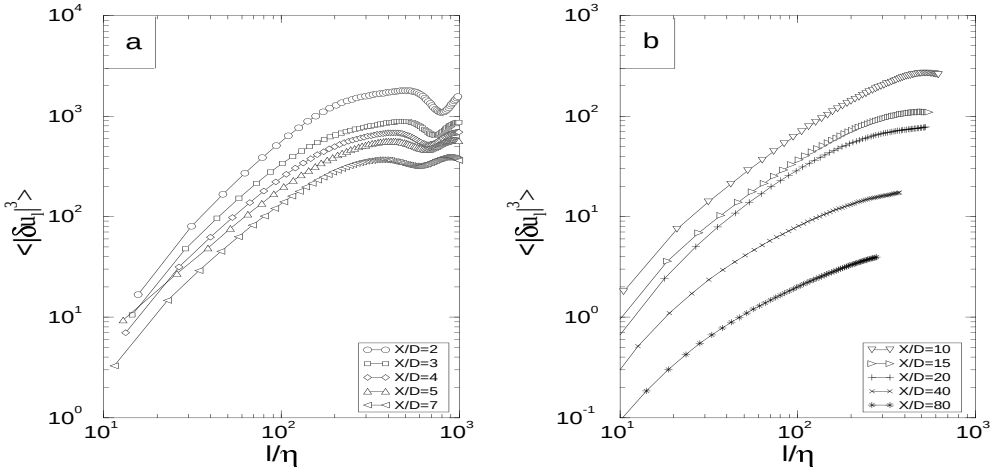

Figure 5.9: Comparison between $\langle \mid \delta u_\ell \mid^3 \rangle$ as a function of ℓ/η, for the lateral plane $Y/D = 0$, at different downstream distances X/D from the cylinder.

To further clarify the absence of proportionality between the two quantities, we have also plotted the ratio $R = \langle \delta u_\ell^3 \rangle / \langle \mid \delta u_\ell \mid^3 \rangle$ as a function of the non-dimensional scale ℓ/η. The results can be seen in figure 5.10 to 5.12. The scaling properties of the two quantities differ strongly at most downstream distances X/D from the cylinder for the three analyzed lateral positions Y/D. It can be seen that the scaling properties of the two quantities differ increasingly in non-homogeneous turbulence, as predicted by Stolovitzky and Sreenivasan (1993). This is a perverse consequence of the use of the absolute values of the velocity increments for studying the odd moments in non-homogeneous turbulent flows. In fact, eacg characteristic refers to distinct statistical information. The change of sign of $\langle \delta u_\ell^3 \rangle$ means that the transfer dynamics is anomalous with respect to a well established cascade (inverse cascade of energy to large scales is quite possible in non-homogeneous flows), whereas $\langle \mid \delta u_\ell \mid^3 \rangle$ is an indication of the balance of the transferred energy at scale ℓ to either larger or to smaller scales. According to the above considerations, which are consequent with the similarity hypothesis described in equation (3.37), we define in what follows the third-order structure function by averaging the absolute values of the velocity increments.

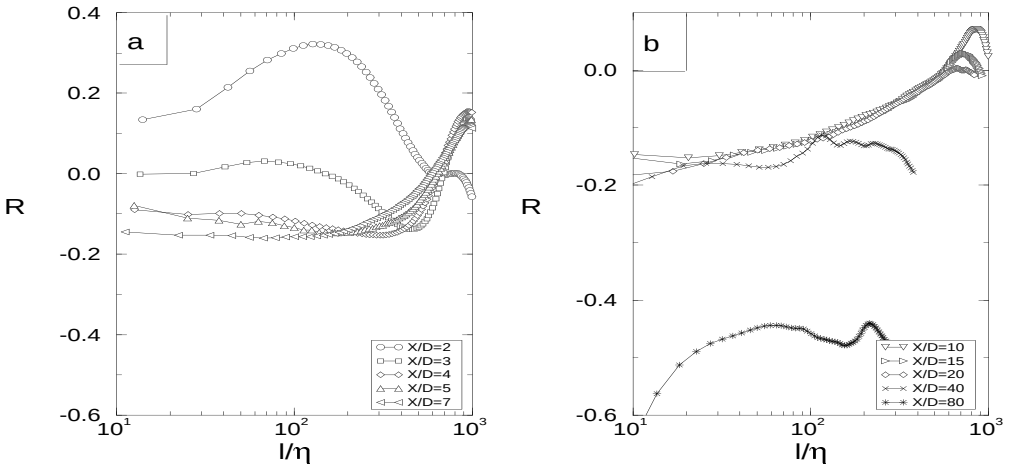

Figure 5.10: Ratio between $\langle \delta u_\ell^3 \rangle$ and $\langle \mid \delta u_\ell \mid^3 \rangle$ as a function of ℓ/η, for the lateral plane $Y/D = -0.8$, at different downstream distances X/D from the cylinder.

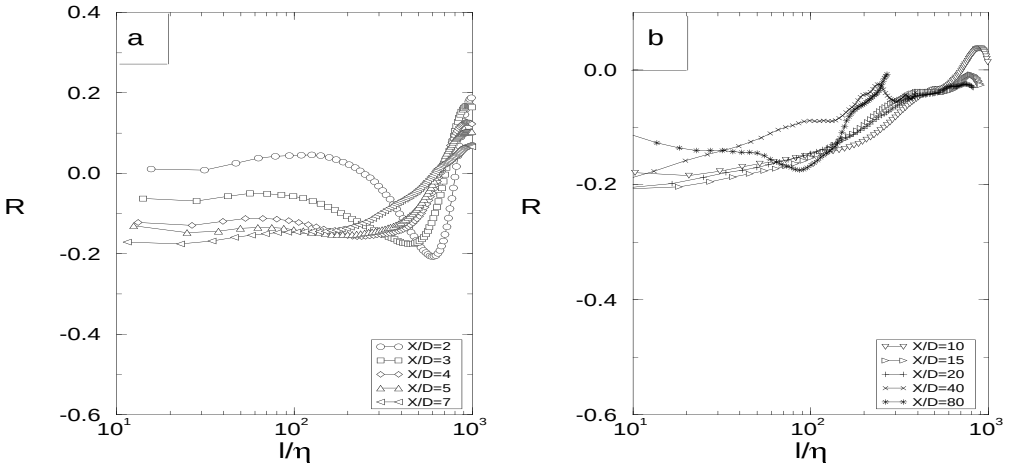

Figure 5.11: Ratio between $\langle \delta u_\ell^3 \rangle$ and $\langle \mid \delta u_\ell \mid^3 \rangle$ as a function of ℓ/η, for the lateral plane $Y/D = -0.4$, at different downstream distances X/D from the cylinder.

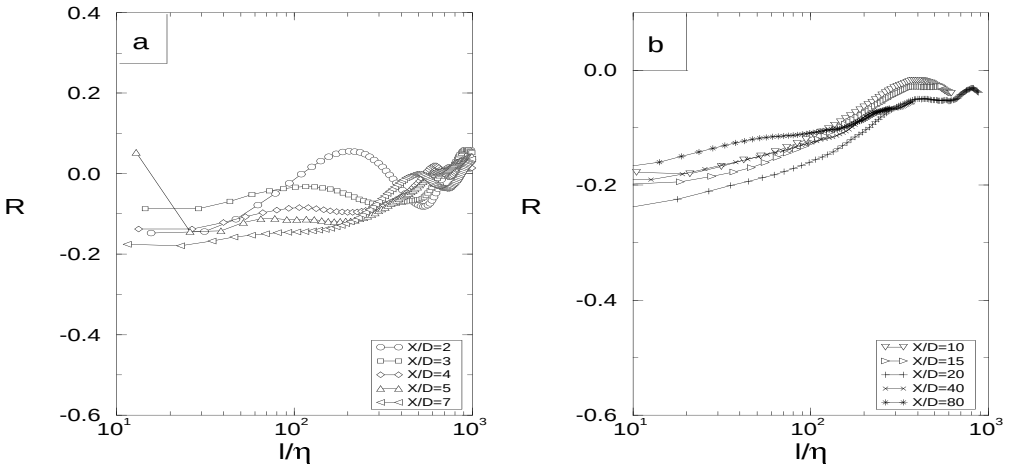

Figure 5.12: Ratio between $\langle \delta u_\ell^3 \rangle$ and $\langle \mid \delta u_\ell \mid^3 \rangle$ as a function of ℓ/η, for the lateral plane $Y/D = 0$, at different downstream distances X/D from the cylinder.

5.3 Absolute scaling exponent

As mentioned in chapter 3, we use the absolute value of the velocity differences for the odd values of p (see equation 3.2), then the absolute scaling exponent ζ_p of the absolute value of the velocity differences is defined as:

$$\zeta_p = \frac{dlog\langle \mid \delta u_\ell \mid^p \rangle}{dlog\ell}, \tag{5.1}$$

where $\langle ... \rangle$ stands for ensemble average and ℓ is the separation distance. The relation (5.1) calculated at each point is more useful than plotting $\langle \mid \delta u_\ell \mid^p \rangle$ versus ℓ/η and defining an average slope, because it shows clearly the region where ζ_p is scale dependent on or scale independent of the separation distance ℓ; this scaling is again a check on the extent of the inertial range.

In homogeneous turbulence, a standard and straightforward procedure in the analysis of the longitudinal structure functions is to select in a log-log plot of $\langle \mid \delta u_\ell \mid^p \rangle$ the interval bounds where the slope for the third order structure function versus ℓ is unity ($\zeta_3 = 1$). This implies self-similar scaling of the third-order structure function, and by extension self-similar scaling of all structure functions. The bounds of this range are taken to be the bounds of the inertial range. The inertial range is physically defined as a range of scales where both the forcing and the dissipation process are irrelevant because they are locally in equilibrium. The existence of an inertial range at scale ℓ demands that ℓ be sufficiently small compared with the integral scale L and sufficiently large compared with the Kolmogorov scale η.

In non-homogeneous flows, ζ_p may also depend on the separation distance ℓ in a complex fashion. Therefore, the fundamental result $\zeta_3 = 1$ of the Kolmogorov theory that allows us to define an inertial range is not observed. This behavior was observed by Babiano *et al.* (1995, 1997) in their numerical experiments for non-homogeneous turbulence.

Investigating this issue, figures 5.13, 5.14 and 5.15 show the longitudinal absolute scaling exponents as a function of non-dimensional scale ℓ/η, at the downstream distances $X/D = 2, 4, 7, 20$ from the cylinder in the lateral positions $Y/D = -0.8$, $Y/D = -0.4$ and $Y/D = 0$, respectively. It is clearly seen in all positions that the absolute scaling exponents ζ_p depend on ℓ, even for ζ_3. In all positions ζ_p is a monotonous decreasing function of ℓ and always $\zeta_p < p$. Hence, the scaling laws of the velocity structure functions cannot be clearly detected following the Kolmogorov theory. This could be considered surprising because the Reynolds number is large enough, so it is apparent that there are two deviations from Kolmogrov's theory (K41) in non-homogeneous flows: the first is that ζ_p is a function of ℓ and the second is that there is no inertial range where $\zeta_3 = 1$. This led us to use an alternative technique in order to determine an inertial scaling range.

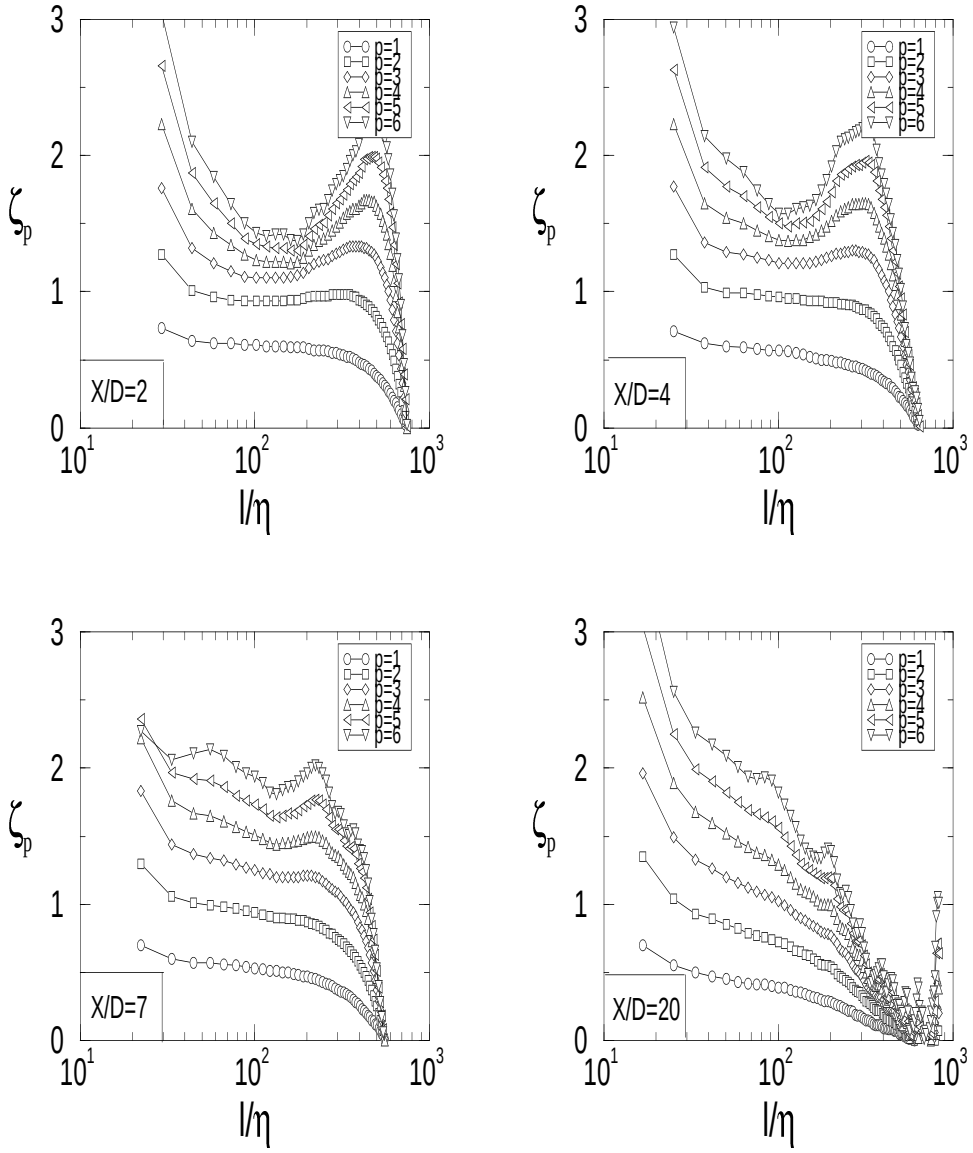

Figure 5.13: Absolute scaling exponents ζ_p as a function of ℓ/η, for the lateral plane $Y/D = -0.8$, at different downstream distances $X/D = 2, 4, 7, 20$ from the cylinder.

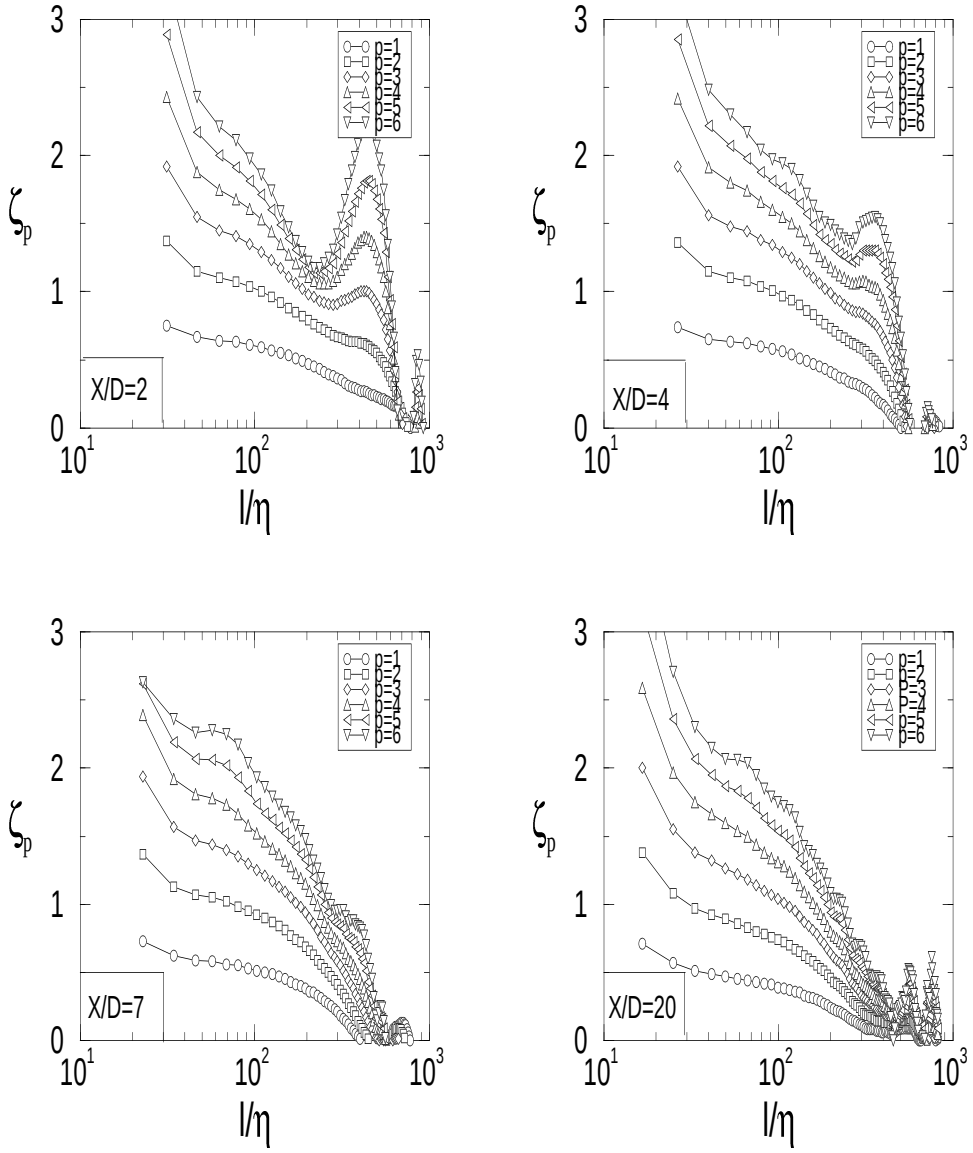

Figure 5.14: Absolute scaling exponents ζ_p as a function of ℓ/η, for the lateral plane $Y/D = -0.4$, at different downstream distances $X/D = 2, 4, 7, 20$ from the cylinder.

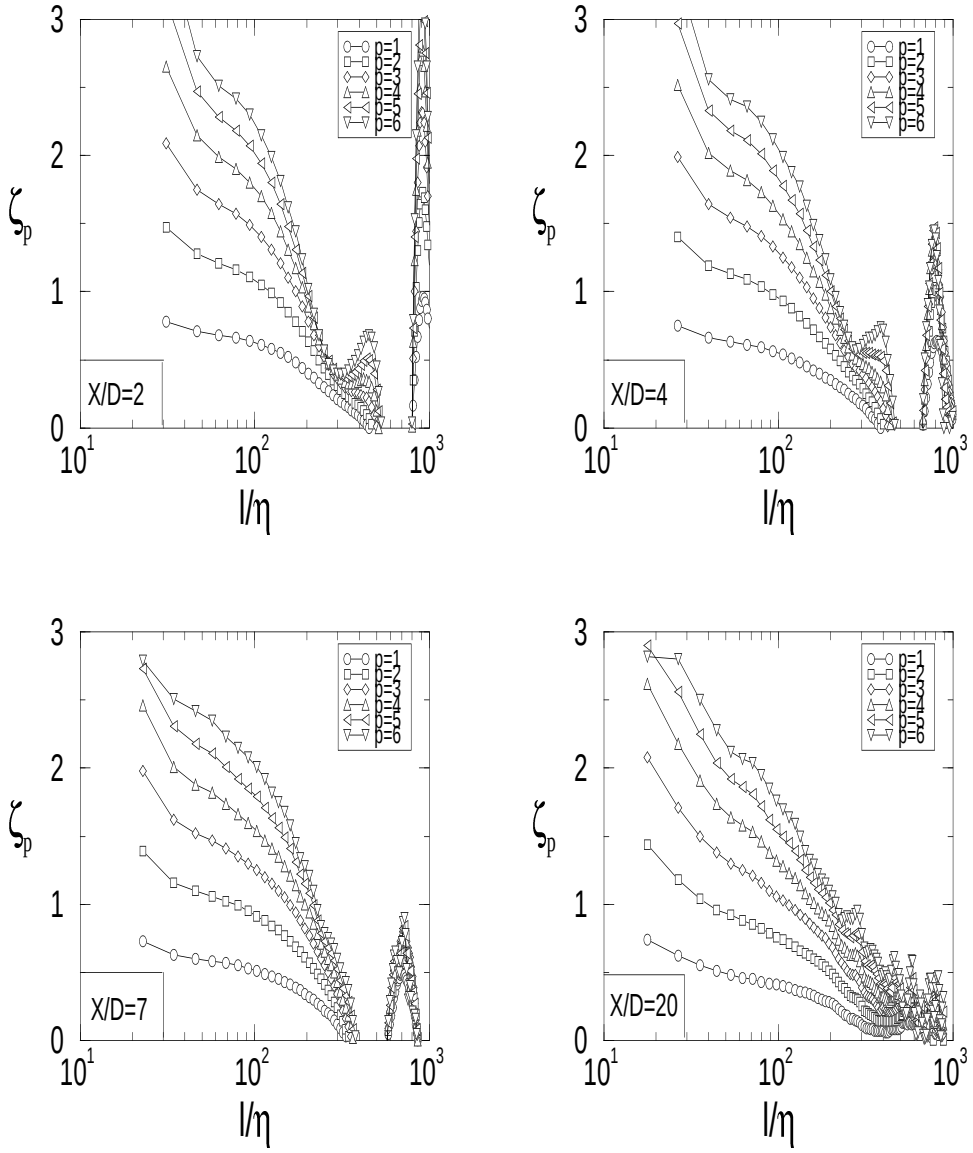

Figure 5.15: Absolute scaling exponents ζ_p as a function of ℓ/η, for the lateral plane $Y/D = 0$, at different downstream distances $X/D = 2, 4, 7, 20$ from the cylinder.

5.4 Relative scaling exponent

Quantitative information on the intermittency effects can be obtained for homogeneous and isotropic turbulence, by the determination of the scaling laws starting with the location of the inertial range using the third-order structure function as mentioned above. In non-homogeneous and non-isotropic turbulence, an inertial range, where the absolute scaling exponent of the third-order structure function should be ζ_3=1, cannot be detected, then, it is not possible to study the scaling behavior in the framework of the Kolmogorov theory as shown by Babiano *et al.* (1995, 1997). Therefore, it is necessary to use the ESS method in order to study the intermittency by means of the relative scaling exponents $\zeta_p/\zeta_3 = \frac{d\log\langle|\delta u_\ell|^p\rangle}{d\log\langle|\delta u_\ell|^3\rangle}$.

As already explained in section 4.3, the scaling ranges can be detected more accurately by plotting the p-order moment of the absolute values of the velocity difference $\langle\mid \delta u_\ell \mid^p\rangle$, with respect to the third order moment of the absolute values of the velocity difference $\langle\mid \delta u_\ell \mid^3\rangle$, or by plotting ζ_p/ζ_3 versus the separation distance ℓ.

Figures 5.16, 5.17 and 5.18 show the longitudinal relative absolute scaling exponents as a function of non-dimensional scale ℓ/η, at the downstream distances $X/D = 2, 4, 7, 20$ from the cylinder in the lateral positions $Y/D = -0.8$, $Y/D = -0.4$ and $Y/D = 0$, respectively. Most of the experiments clearly show a range where the relative scaling exponents ζ_p/ζ_3 are practically scale-invariant. On the other hand, the values of ζ_p/ζ_3 are not the same at all the downstream distances. Near the source of turbulence the ESS scaling range is shorter than far from the source of turbulence. This can be explained by noting that near the source of, turbulence is not fully developed and locally non-homogeneous and non-isotropic. In contrast, far from the cylinder the flow becomes quasi homogeneous and isotropic. This behavior was also detected by Gaudin *et al.* (1998). They plotted the plotted the spatial distribution of the relative scaling exponents behind the cylinder.

Moreover, our results show that ESS works even when a strong mean shear is present, such as in the near wake behind a cylinder at the downstream distance $X/D = 2$. This result contradicts Benzi *et al.* (1996), who assumed that ESS does not work in situations when a strong mean shear is present, such as in the shear behind a cylinder and in the boundary layer turbulence. However, ESS may be more robust than the usual self-similar scaling with respect to ℓ predicted by Kolmogorov (1941) in the definition of an inertial range, even in the presence of non-homogeneity and non-isotropy of the flow, as we will see in the following sections.

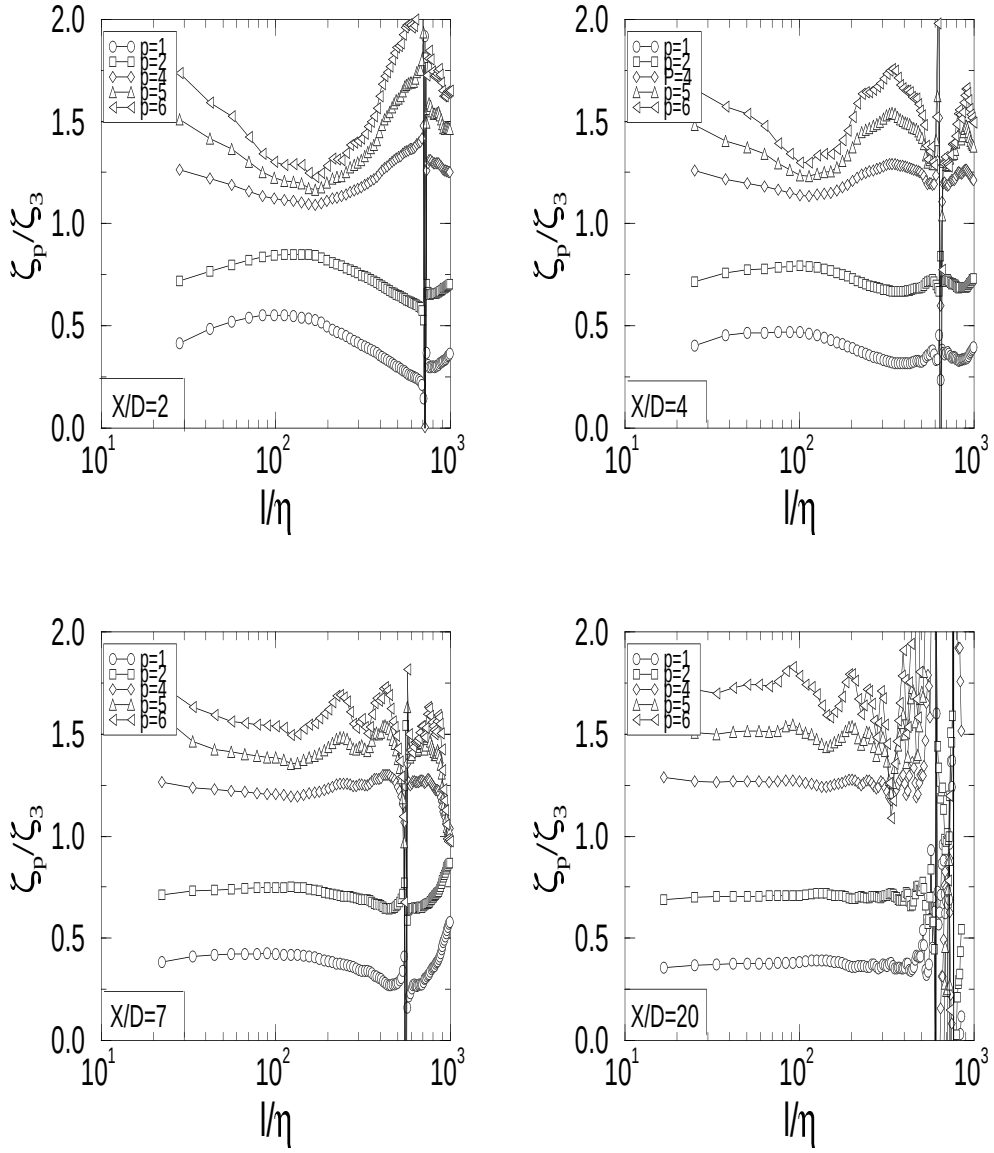

Figure 5.16: Relative scaling exponents ζ_p/ζ_3 as a function of ℓ/η, for the lateral plane $Y/D = -0.8$, at different downstream distances $X/D = 2, 4, 7, 20$ from the cylinder.

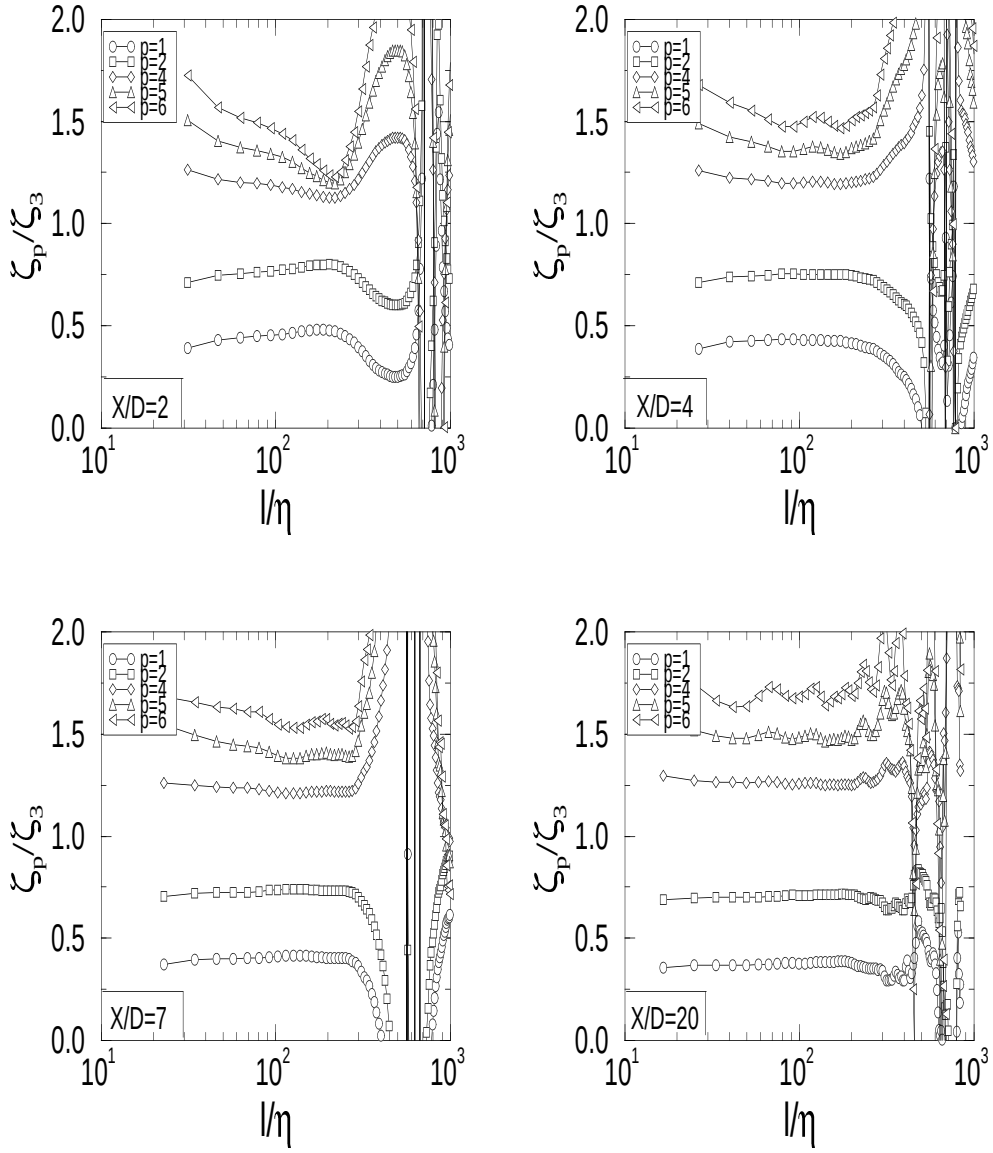

Figure 5.17: Relative scaling exponents ζ_p/ζ_3 as a function of ℓ/η, for the lateral plane $Y/D = -0.4$, at different downstream distances $X/D = 2, 4, 7, 20$ from the cylinder.

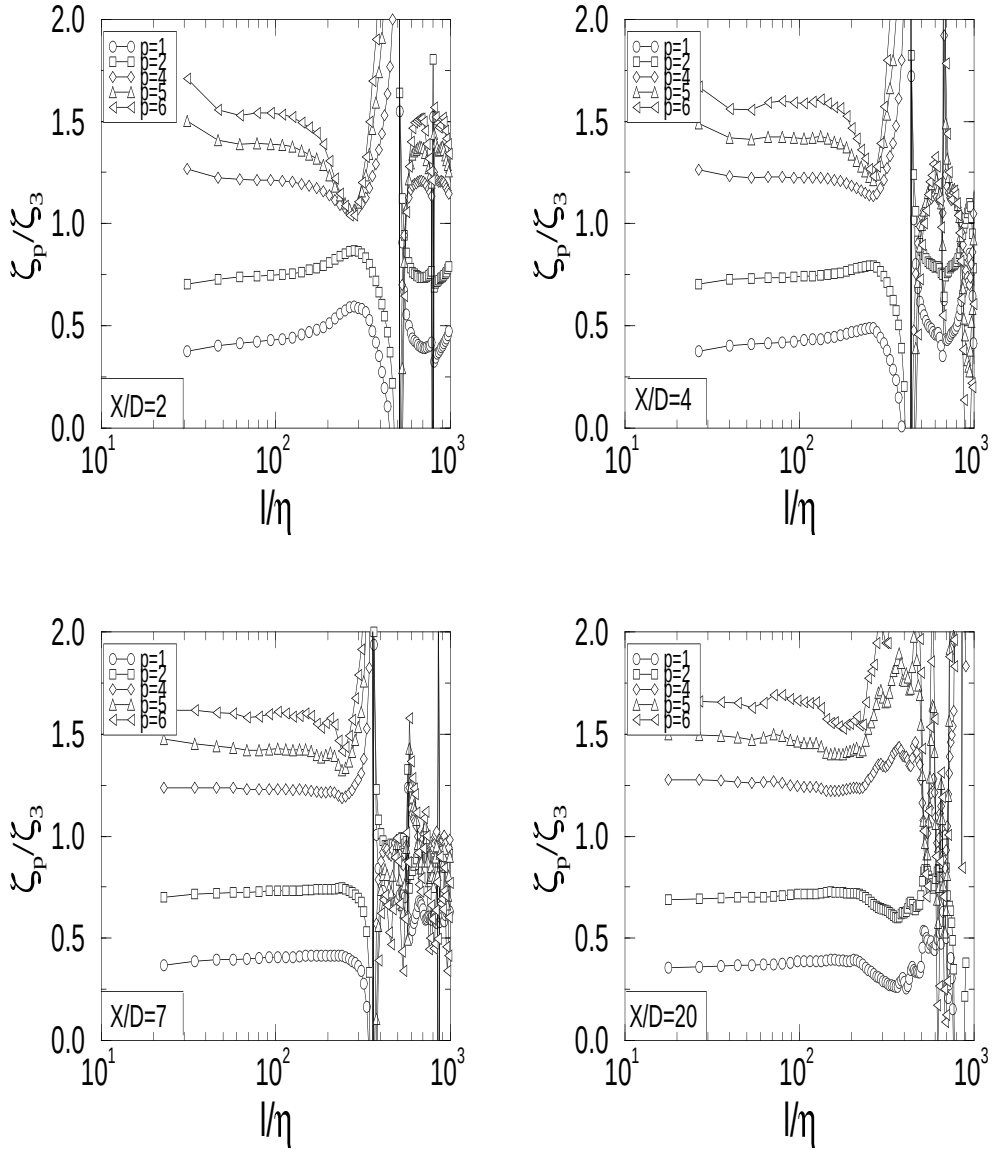

Figure 5.18: Relative scaling exponents ζ_p/ζ_3 as a function of ℓ/η, for the lateral plane $Y/D = 0$, at different downstream distances $X/D = 2, 4, 7, 20$ from the cylinder.

5.5 Behavior of ζ_3, $(\delta_\infty - \delta_0)$ and Δ

The experimental illustrations of the behavior of ζ_3 as a function of non-dimensional scale ℓ/η at the downstream distance $X/D = 2, 3, 4, 5, 7, 10, 15, 20$ for the lateral positions $Y/D = -0.8$, $Y/D = -0.4$ and $Y/D = 0$, respectively are reported in figures 5.19, 5.20 and 5.21. The curves clearly demonstrate the anomalous behavior of the third-order structure function. It is appropriate to emphasize the results corresponding to the position $Y/D = -0.8$ just outside the cylinder radius. Near the cylinder, where the flow dynamics is nonlocal and strongly non-homogeneous, ζ_3 shows maximum average values. Further downstream, ζ_3 decreases to a minimum closer to 1, which corresponds to the most remote explored regions in the cylinder wake. At such distances, the turbulence displays quasi-homogeneous properties and a local energy spectrum law close to $-5/3$. The decrease of ζ_3 is linked to the transition from nonlocal dynamics to local dynamics along the cylinder wake as the turbulence develops.

To explore the behavior of $(\delta_\infty - \delta_0)$ discussed in chapter 4 it is necessary to compute the contour integral as a function of length-scale ℓ, which figures in the basic definition (3.10) after previous measurement of the longitudinal and transversal components of the velocity and the pressure in the entire flow domain. Until now, this procedure has been conceivable only in the framework of numerical experiments. In the framework of the detailed laboratory measurements analyzed here, the absolute scale-to-scale energy transfer σ_ℓ is approximated by:

$$\sigma_l^* \approx \frac{1}{\ell} < |u^3(\vec{x} + \vec{\ell}) - u^3(\vec{x})| >, \tag{5.2}$$

where $< . >$ now refers to the time average using Taylor's hypothesis locally to obtain the spatial dependence. Clearly, as we have already noticed, the evaluation (5.2) constitutes a rough approximation. First, the contributions to the transfer of the transverse velocity and the work of pressure forces are neglected. Secondly, the approximation (5.2) indeed implies that contour integration in the rigorous definition (3.10) is not performed. Nevertheless, this approximation seems plausible because near the cylinder, where the spectrum behavior is steeper than $k^{-5/3}$, the transversal components of velocity do not contribute to σ_ℓ as $B = 3A$ (Babiano (2000)), on the other hand further away from the cylinder the flow homogenizes and $\sigma_\ell = \sigma_\ell^*$.

Assuming the experimentally convenient approximation (5.2), we shall analyze the scaling properties of the hierarchy

$$H^*(p, \ell, t) = \frac{< \sigma_\ell^{*p+1} >}{< \sigma_\ell^{*p} >}, \tag{5.3}$$

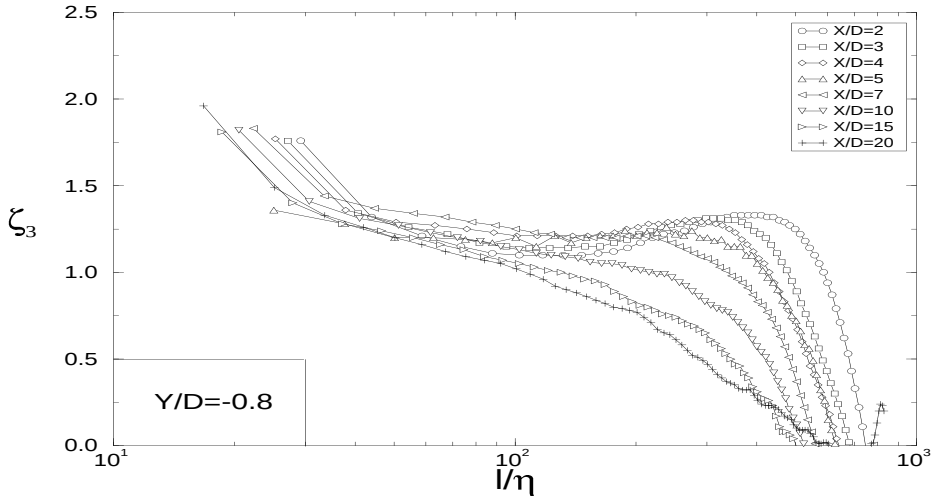

Figure 5.19: Third order absolute scaling exponent ζ_3 as a function of ℓ/η, for the lateral plane $Y/D = -0.8$, at different downstream distances X/D from the cylinder.

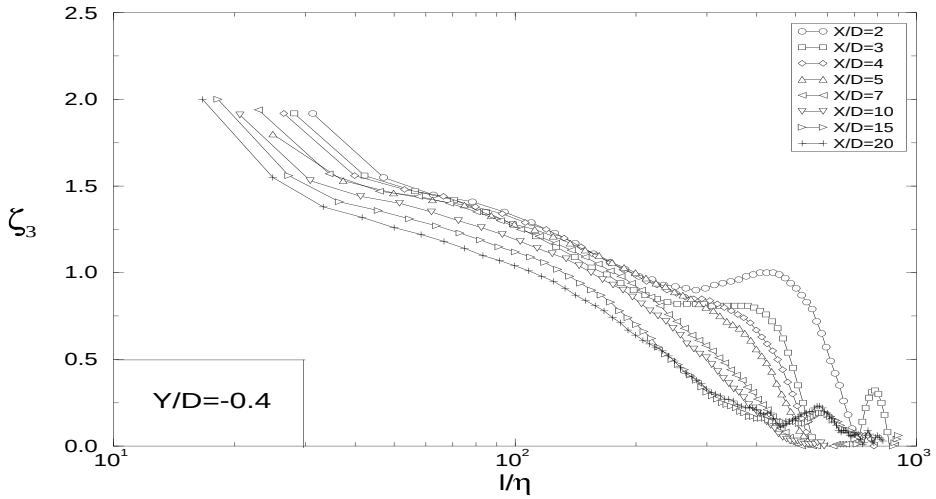

Figure 5.20: Third order absolute scaling exponent ζ_3 as a function of ℓ/η, for the lateral plane $Y/D = -0.4$, at different downstream distances X/D from the cylinder.

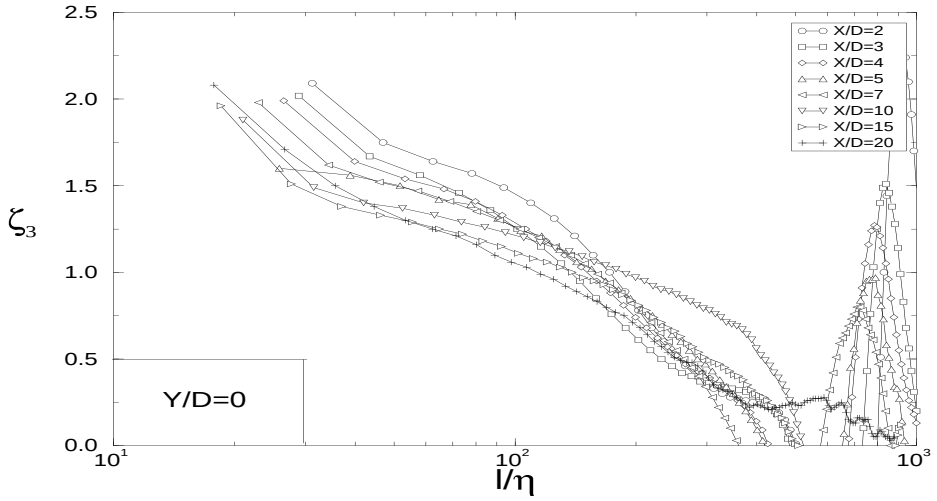

Figure 5.21: Third order absolute scaling exponent ζ_3 as a function of ℓ/η, for the lateral plane $Y/D = 0$, at different downstream distances X/D from the cylinder.

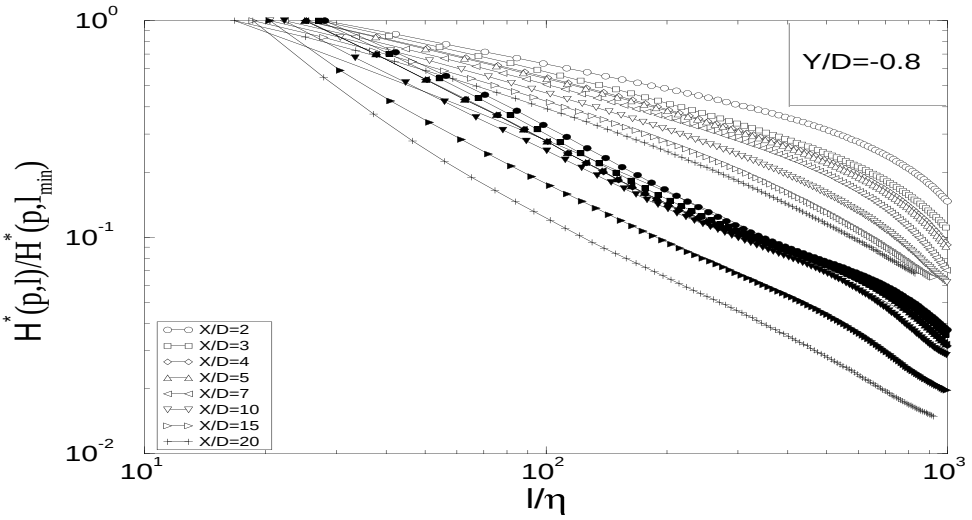

Figure 5.22: Variation of hierarchy $H^*(p,\ell)/H^*(p,\ell_{min})$ for $p = 0$ and $p = 5$ as a function of ℓ/η, for the lateral plane $Y/D = -0.8$, at different downstream distances X/D from the cylinder.

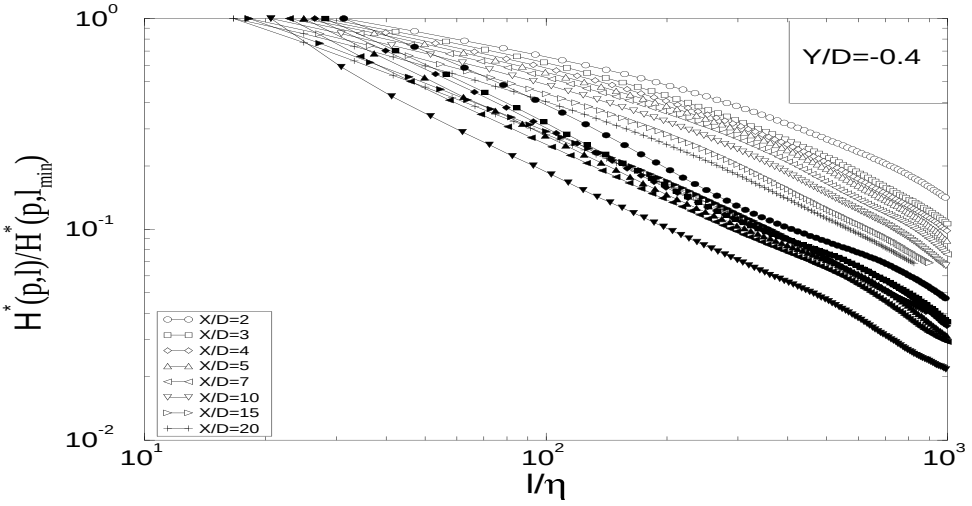

Figure 5.23: Variation of hierarchy $H^*(p,\ell)/H^*(p,\ell_{min})$ for $p = 0$ and $p = 5$ as a function of ℓ/η, for the lateral plane $Y/D = -0.4$, at different downstream distances X/D from the cylinder.

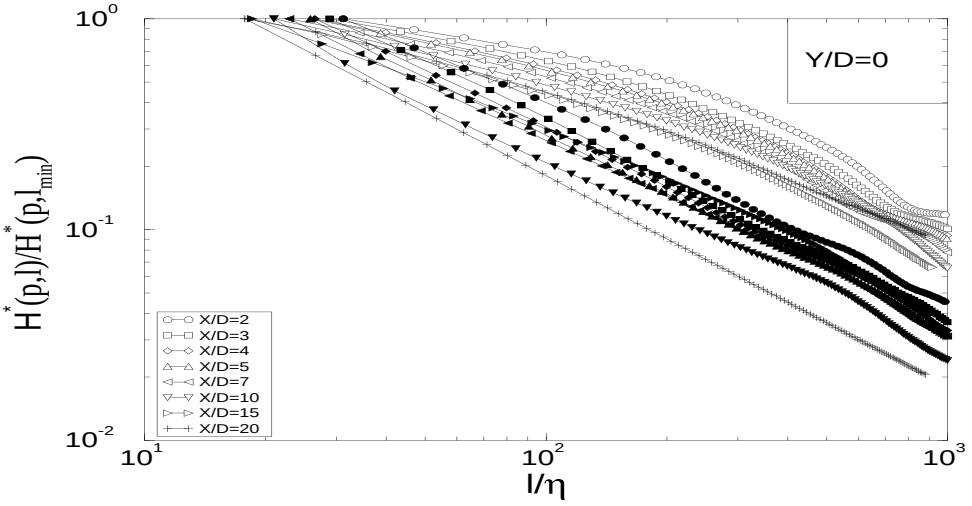

Figure 5.24: Variation of hierarchy $H^*(p,\ell)/H^*(p,\ell_{min})$ for $p = 0$ and $p = 5$ as a function of ℓ/η, for the lateral plane $Y/D = 0$, at different downstream distances X/D from the cylinder.

and we shall denote the corresponding local scaling exponents δ_0^* and δ_∞^*, by analogy with (3.30) and (3.31). In this case we have a similar definition to (3.42), $\Delta^* = (\delta_\infty^* - \delta_0^*)/\zeta_3$. Figures 5.22, 5.23 and 5.24 show the hierarchy (5.3) for $p = 0$ (open symbols) and $p = 5$ (filled symbols) as a function of non dimensional length-scale ℓ/η for all the explored positions near the cylinder, up to $X/D = 20$, corresponding to the section $Y/D = -0.8$, $Y/D = -0.4$ and $Y/D = 0$, respectively. This is the most interesting region where the dynamics is nonlocal, and ζ_3 decays, as pointed out in figures 5.19, 5.20 and 5.21.

The hierarchy (5.3) is normalized by its corresponding values at the smallest scales explored. The decreasing behavior of the hierarchy for $p = 0$ (open symbols) indicates that the variance of the energy transfer increases when the dynamics becomes nonlocal near the cylinder. Near the cylinder, the steepest δ_0^* shows a minimum at all length-scales ℓ/η and saturates far from the cylinder. At the same time, δ_∞^* remains almost stationary. In other words, $(\delta_\infty^* - \delta_0^*)$ is maximum near the cylinder where the flow dynamics is strongly nonlocal. Subsequently, it decreases progressively to a minimum saturation value far away from the cylinder, where the dynamics tends to be local. This same behavior is observed in numerical experiments reported in Babiano (2000). It seems that the approximations (5.2) and (5.3) assumed here do not change this remarkable behavior.

Figures 5.25, 5.26 and 5.27 show Δ^* as a function of the non-dimensional scale ℓ/η for the three lateral distances $Y/D = -0.8$, $Y/D = -0.4$ and $Y/D = 0$ at different downstream distances X/D from the cylinder up to $X/D = 20$. The quantity Δ^* shows good scale-invariance, even when both the absolute scaling exponents ζ_3 and $(\delta_\infty^* - \delta_0^*)$ clearly depend on the separation distance ℓ/η. This scale-invariance of Δ^* appears as a result of the compensation effect which operates in (3.42) between $(\delta_\infty^* - \delta_0^*)$ and ζ_3 , thus explaining and consolidating the ESS property even in non-homogeneous flows. The most important observation is that the value of Δ^* does not depend on the separation distance ℓ. These results are entirely consistent with a numerical investigation of non-homogeneous two-dimensional turbulence performed by Babiano *et al.* (1997), Babiano (2000) and other experiments reported by Mahjoub *et al.* (2000a), and reinforces the idea that both the unmasked properties in non-homogeneous flows and the proposed tool are well sustained irrespective of the particular flow geometry. Here, we have neglected the contribution to the energy transfer of the lateral structure of the velocity field and the work of pressure forces. Neither this approximation nor Taylor's hypothesis apparently modifies the statistical link in Δ^*, since our estimate Δ^* is close to Δ of equation (3.42), where all contributions to the energy transfer were considered. Clearly, this is *a posteriori* argument, which must be confirmed on the basis of more consistent experimental investigations of the turbulent wake behind a cylinder, including measurements of the pressure and the transversal structure of the velocity field.

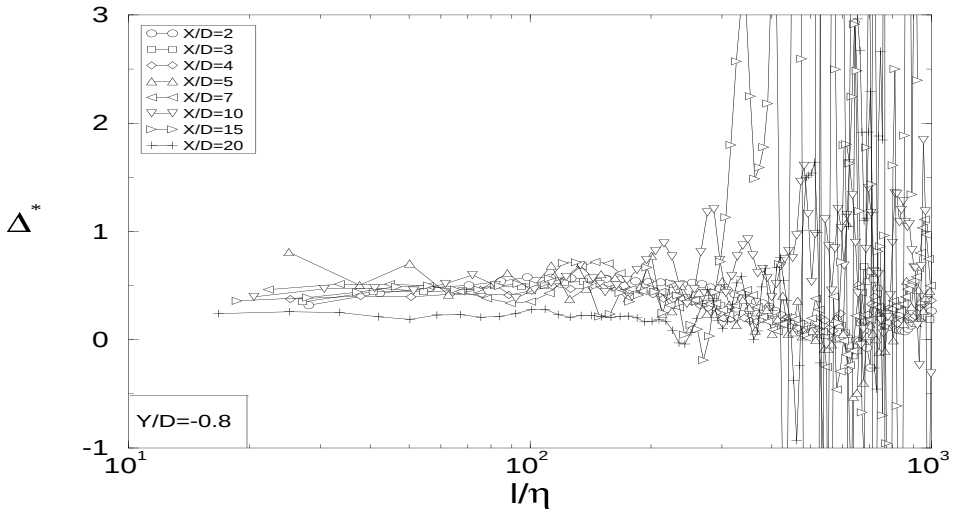

Figure 5.25: Dependence of Δ^* on non-dimensional scale ℓ/η, for the lateral plane $Y/D = -0.8$, at different downstream distances X/D from the cylinder.

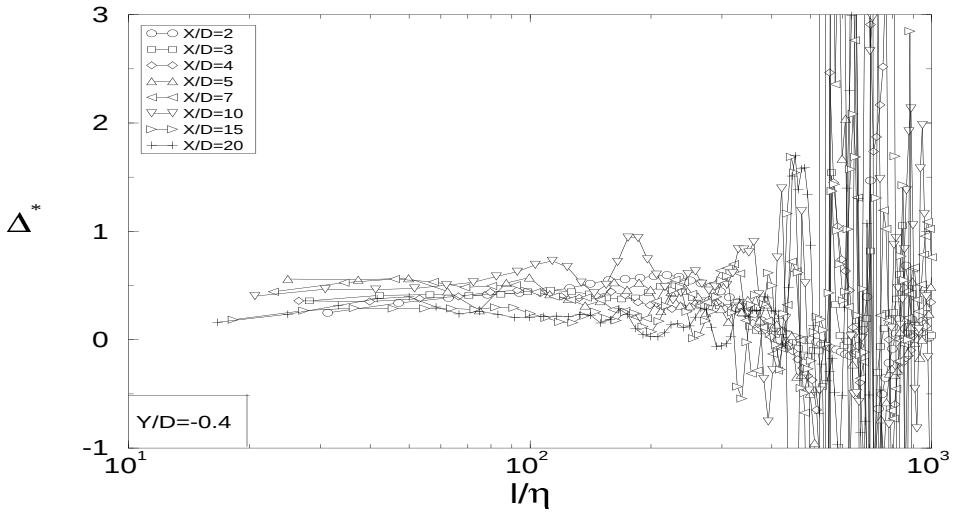

Figure 5.26: Dependence of Δ^* on non-dimensional scale ℓ/η, for the lateral plane $Y/D = -0.4$, at different downstream distances X/D from the cylinder.

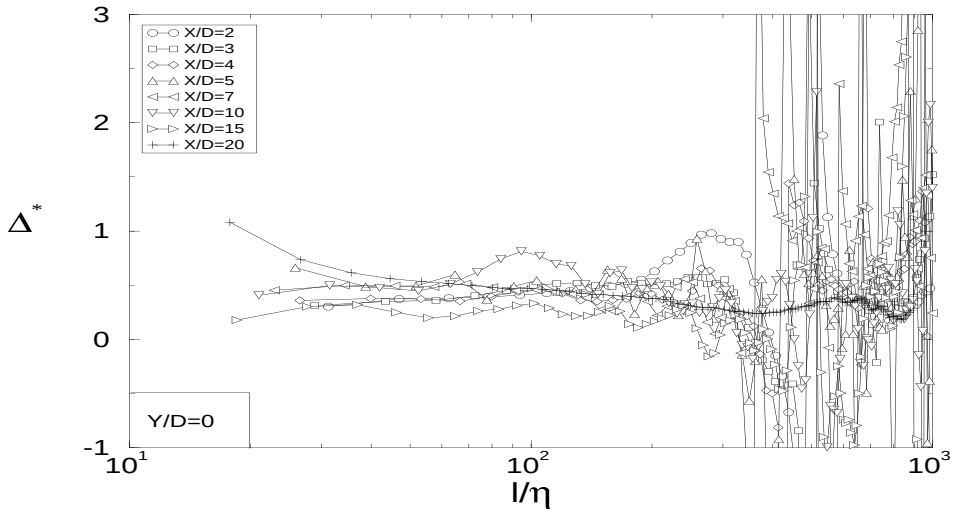

Figure 5.27: Dependence of Δ^* on non-dimensional scale ℓ/η, for the lateral plane $Y/D = 0$, at different downstream distances X/D from the cylinder.

5.6 Intermittency

In this section we have used two methods to measure the intermittency in the turbulent wake flow. The first was the intermittency parameter μ calculated using the relation (2.24) and replacing the sixth-order scaling exponent ξ_6 by the relative scaling exponent ζ_6/ζ_3. The second was the intermittency parameter β calculated from the relation (3.43) of the SL model. The two methods are now compared.

5.6.1 Intermittency parameter μ

Figure 5.28 illustrates the behavior of the intermittency parameter μ as a function of the downstream distance X/D form the cylinder for the three lateral distances $Y/D = -0.8$, $Y/D = -0.4$ and $Y/D = 0$. It appears that the intermittency parameter depends on the location in the flow and decreases with the downstream distance from the cylinder, which agrees with the results of the relative scaling exponents that were found to deviate strongly from the K41 theory near the cylinder wake. In all the locations in the wake flow μ is greater than 0.2, the value found by Antonia *et al.* (1982) in homogeneous and isotropic flows.

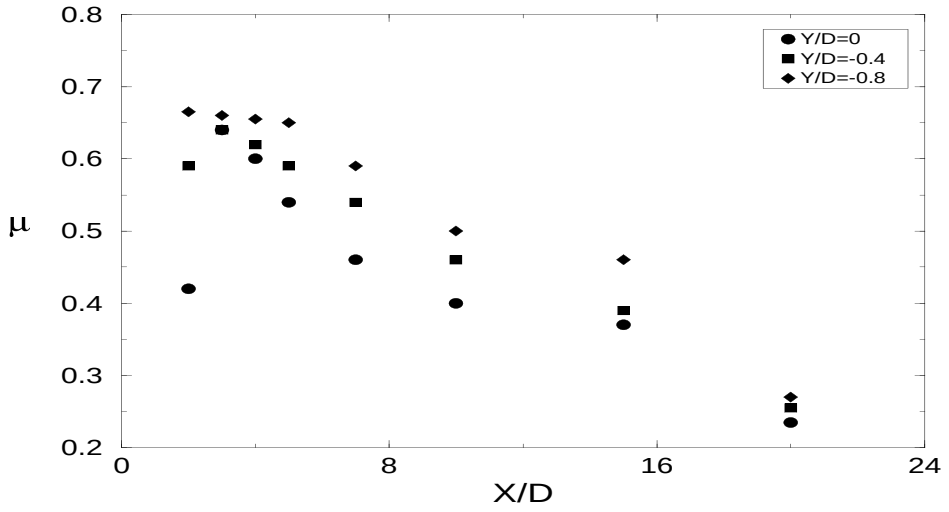

Figure 5.28: Variation of the intermittency parameter μ with the downstream distance X/D from the cylinder at three lateral distances $Y/D = -0.8$, $Y/D = -0.4$ and $Y/D = 0$.

5.6.2 Intermittency parameter β

We have evaluated the contribution of $I(p/3)$ to the relative scaling exponents ζ_p/ζ_3 in (3.41) assuming $h = exp(-ap)$ and $a = -h'(0)$. Moreover, we assume that $I(p/3)$ follows the relationship proposed in the SL model (1994) detailed in equation (3.43).

Figures 5.29, 5.30 and 5.31 show the behavior of β as a function of downstream distance up to $X/D = 20$ for three lateral positions which are representative of the wake: $Y/D = -0.8$, $Y/D = -0.4$ and $Y/D = 0$. The variation of the intermittency parameter β with downstream distance X/D near the cylinder is apparent. The way in which β is calculated will depend on the order of the structure function. This parameter was computed using equations (3.41) and (3.42) with the experimental data for ζ_p/ζ_3 assuming $\Delta = 2/3$. We observe that β depends on the position in the turbulent wake, but it is also important to note that there is a strong dependence on p near the cylinder. This appears as an important limitation of the She-Leveque relation (3.43) in the strongly non-homogeneous case. We see that at about eight cylinder diameters the wake has developed sufficiently as to show similar values of the intermittency in its core. The strong variations occur near the cylinder where the wake is dominated by the coherent structures. These results indicate that β is a more useful tool to measure the intermittency in non-homogeneous flows than μ.

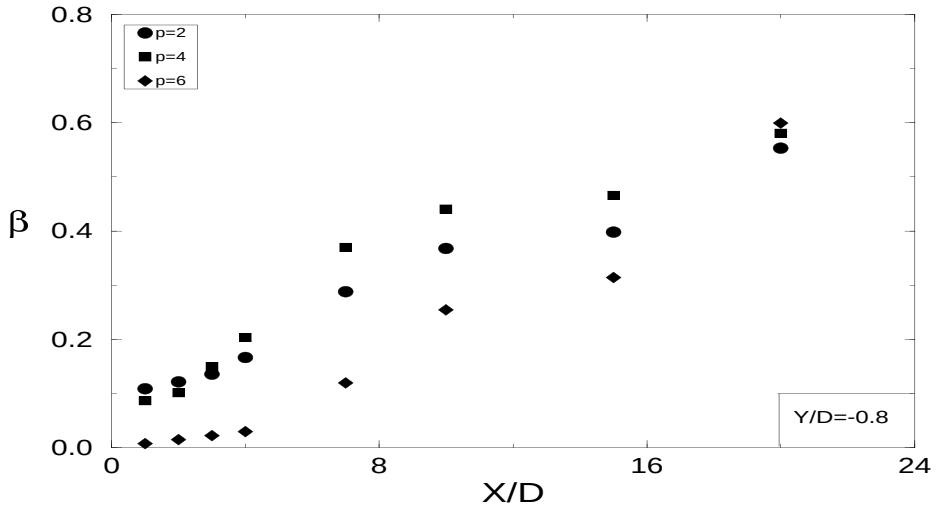

Figure 5.29: Variation of the intermittency parameter β with the downstream distance X/D from the cylinder at the lateral distance $Y/D = -0.8$.

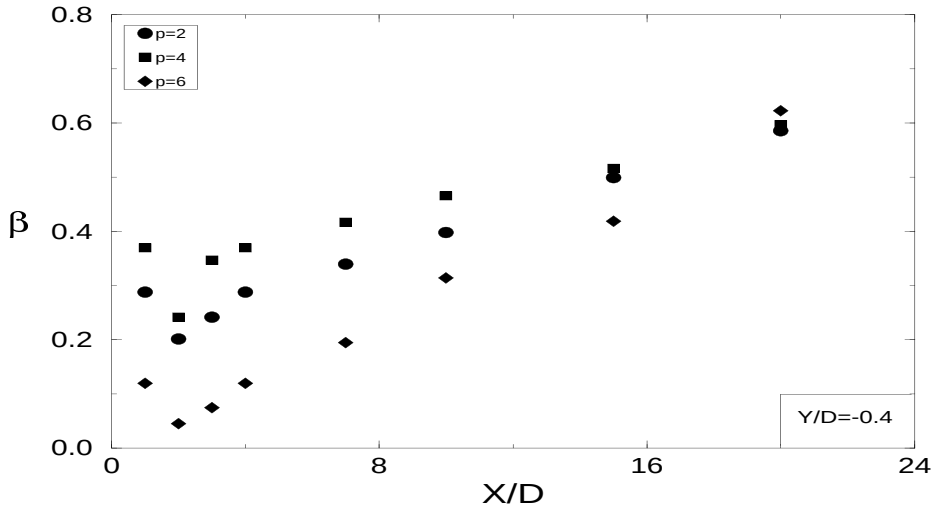

Figure 5.30: Variation of the intermittency parameter β with the downstream distance X/D from the cylinder at the lateral distance $Y/D = -0.4$.

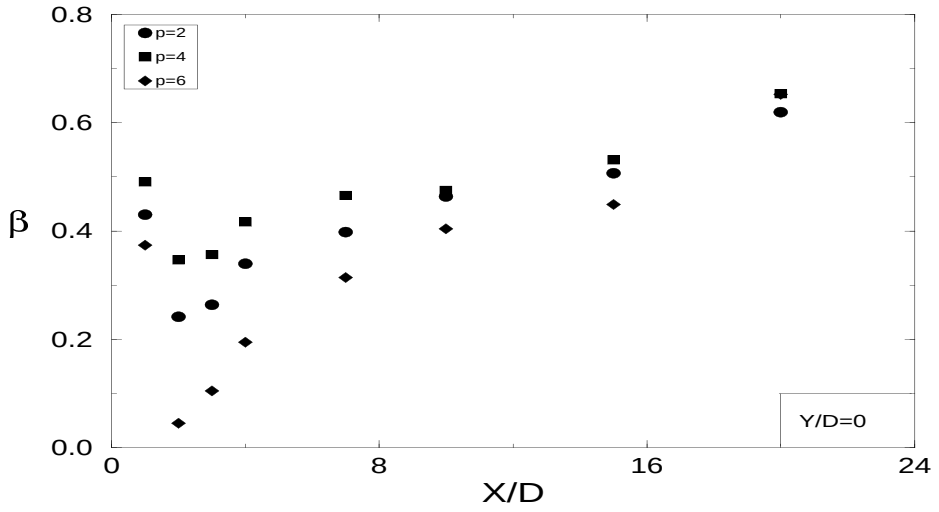

Figure 5.31: Variation of the intermittency parameter β with the downstream distance X/D from the cylinder at the lateral distance $Y/D = 0$.

5.7 Probability distribution functions

To derive the probability distribution functions of any random-field u, it is necessary to calculate the averages $\langle u \rangle$ and standard deviations σ_u of the random-field. In this way, one can easily analyze and compare their statistical properties with other distributions such as Gaussian or exponential distribution. For a Gaussian distribution we have,

$$F(u) = \frac{1}{\sigma_u \sqrt{2\pi}} exp\Big(- \frac{1}{2} \frac{(u - \langle u \rangle)^2}{\sigma_u^2} \Big), \tag{5.4}$$

whereas the exponential distribution is defined as:

$$G(u) = \frac{1}{2\langle u \rangle} exp(- \mid u \mid / \langle u \rangle), \tag{5.5}$$

where $\langle ... \rangle$ stands for ensemble average. The PDFs are best plotted logarithmically versus δu_ℓ. Measurements of PDFs of velocity differences δu_ℓ for fully developed turbulence were obtained from experimental and numerical data (Anselmet *et al.* (1984), Frisch (1995) and Vincent and Meneguzzi (1991)). All of these studies demonstrated that the PDFs of velocity differences depend on the scale ℓ, which is

linked to the usual intermittency phenomenon. The PDF of the velocity differences departs from a Gaussian distribution in the inertial range. At small scales $P(\delta u_\ell)$ has wide, almost exponential tails and at large scales $P(\delta u_\ell)$ has a Gaussian shape.

Figures 5.32, 5.33 and 5.34 show the scale evolution of the PDFs of the longitudinal velocity differences δu_ℓ as a function of the standard deviation of their velocity differences, for three different separation distances ℓ, for cylinder wake turbulence at the downstream distances $X/D = 2$ and $X/D = 20$ respectively with 10^6 samples. In the figures the equivalent Gaussian distributions are plotted for comparison. The figures show that the distributions of the longitudinal velocity differences $P(\delta u_\ell)$ evolve systematically with varying separation distance ℓ. One can also observe that the PDFs are different from the Gaussian distributions for all scales ℓ with large wings, which indicates that strong events have a greater probability of occurrence than a Gaussian event. At both downstream distances the PDF can be divided into two regions: the left region associated with negative velocity differences and the right region associated with positive velocity differences. At location $X/D = 2$ $P(\delta u_\ell)$ has the maximum value at positive velocity differences δu_ℓ, while at location $X/D = 20$ $P(\delta u_\ell)$ has the maximum value at negative velocity differences δu_ℓ. On the other hand, it shown that when the separation distance ℓ increases, the maximum value of $P(\delta u_\ell)$ decreases. For example in figure 5.34 for plane $Y/D = 0$, $P(\delta u_\ell)$ varies from 0.12 to 0.05 for $\ell/\eta = 27$ and $\ell/\eta = 96$ at the location $X/D = 2$, and from 0.11 to 0.08 for $\ell/\eta = 18$ and $\ell/\eta = 64$ at the location $X/D = 20$.

In both locations, the asymmetry is more pronounced at small scales ℓ. The longitudinal probability density function $P(\delta u_\ell)$ clearly shows strong deviations from Gaussian (Kolmogorov (1941)) and quasi-Gaussian (Kolmogorov (1962)) distributions. The PDF of the velocity differences does not depend on the scale ℓ at location $X/D = 2$, while at $X/D = 20$ it depends on scale ℓ. These deviations from Gaussianty and asymmetry are more pronounced at location $X/D = 2$ than at $X/D = 20$ due to the strong non-homogeneity of the flow near the cylinder. The intermittency is greater at location $X/D = 2$ than at $X/D = 20$, which confirms the result of intermittency parameter β obtained in the previous section. This explains why the wake flow seems more contaminated by strong events caused by vortex dynamics generated by the cylinder, related to the formation of these scales, and their interactions. This finding indicates that the deviations from the Gaussian distributions in non-homogeneous flows are not linked to the intermittency but to the non-local dynamics in these flows.

This type of behavior agrees with the results of Gaudin *et al.* (1998) concerning the relative scaling exponents found to be more intermittent in locations near the cylinder than far from it.

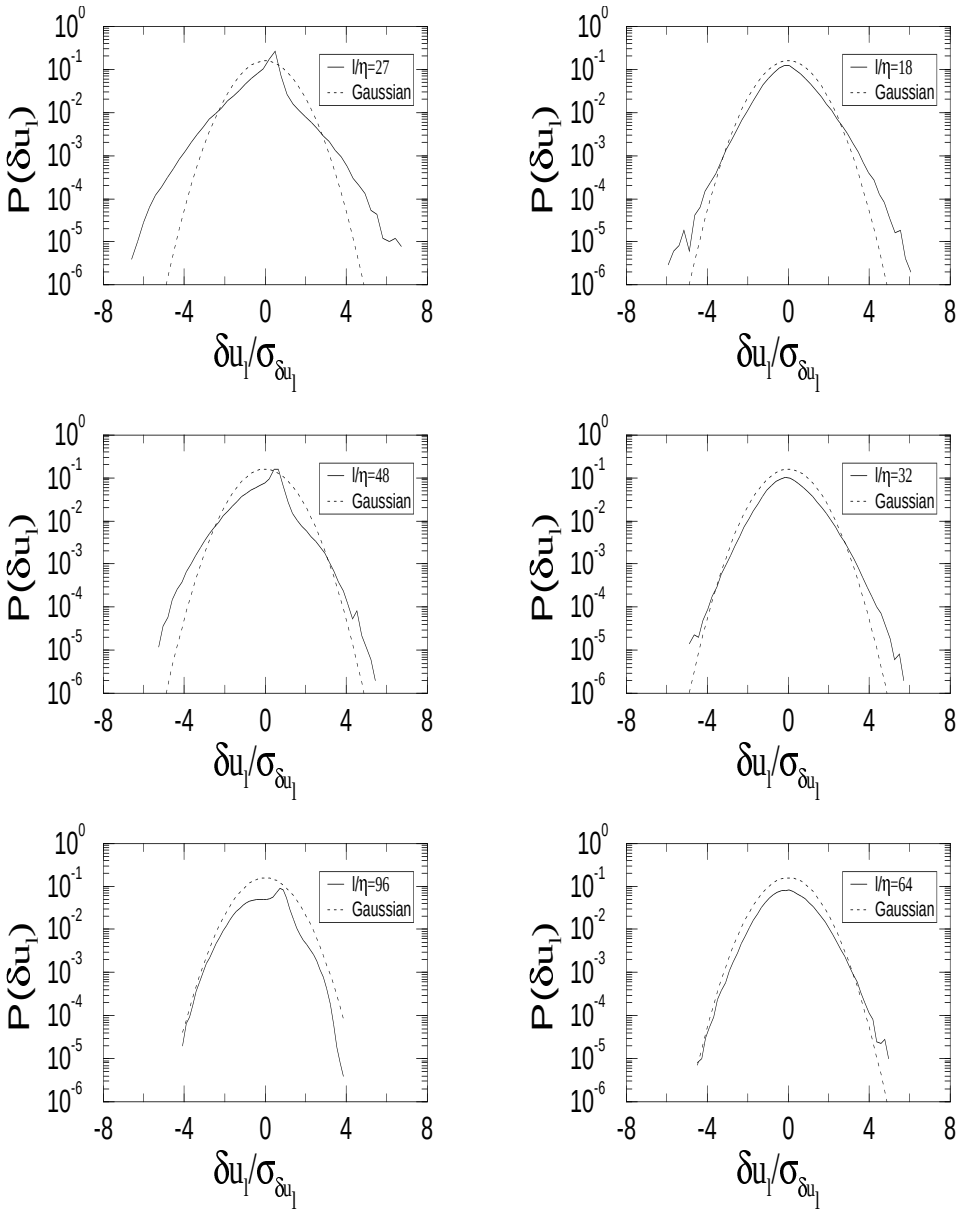

Figure 5.32: The probability distribution function for cylinder turbulence, for the lateral plane $Y/D = -0.8$ and for different ℓ/η, at downstream distances $X/D = 2$ and $X/D = 20$.

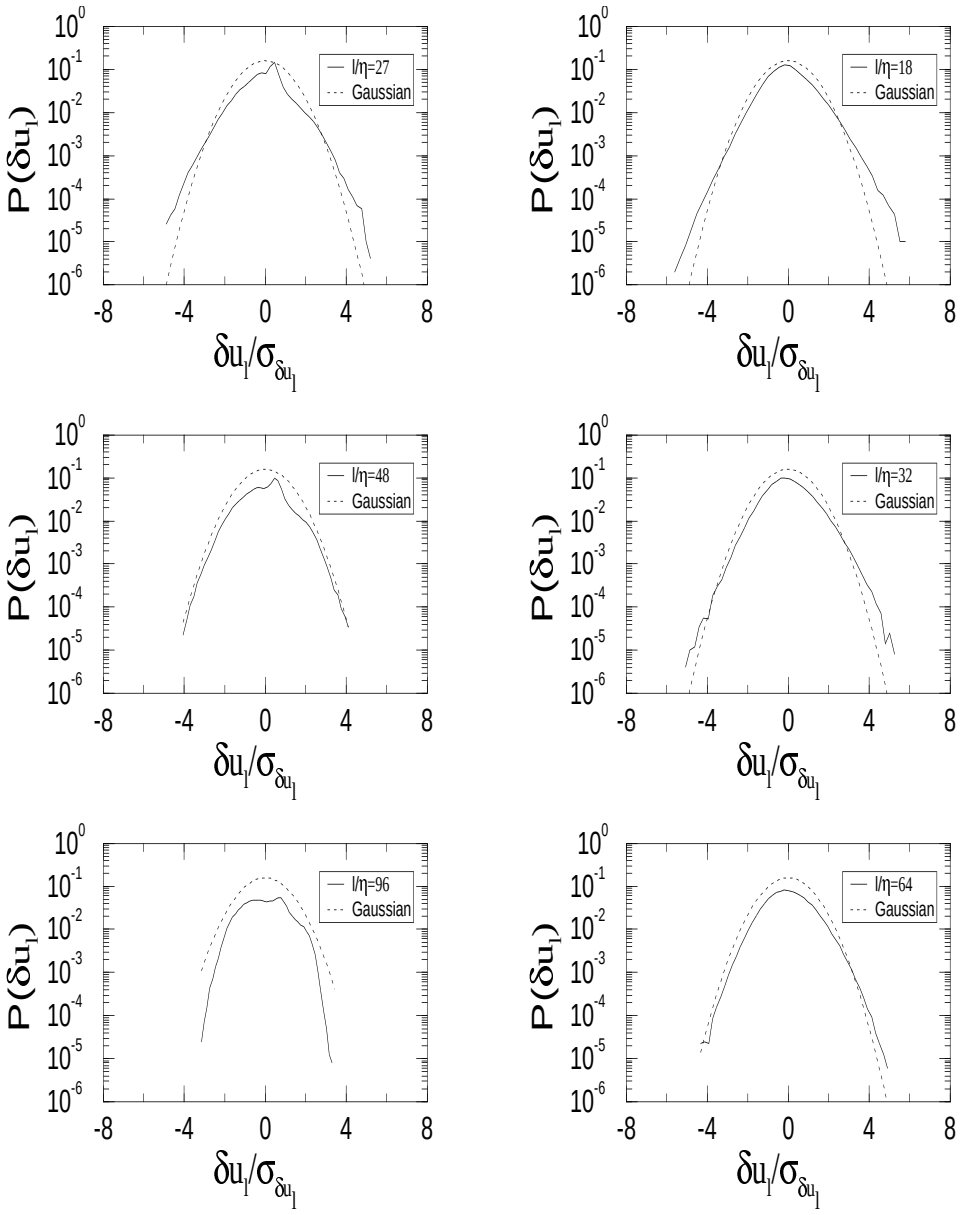

Figure 5.33: The probability distribution function for cylinder turbulence, for the lateral plane $Y/D = -0.4$ and for different ℓ/η, at downstream distances $X/D = 2$ and $X/D = 20$.

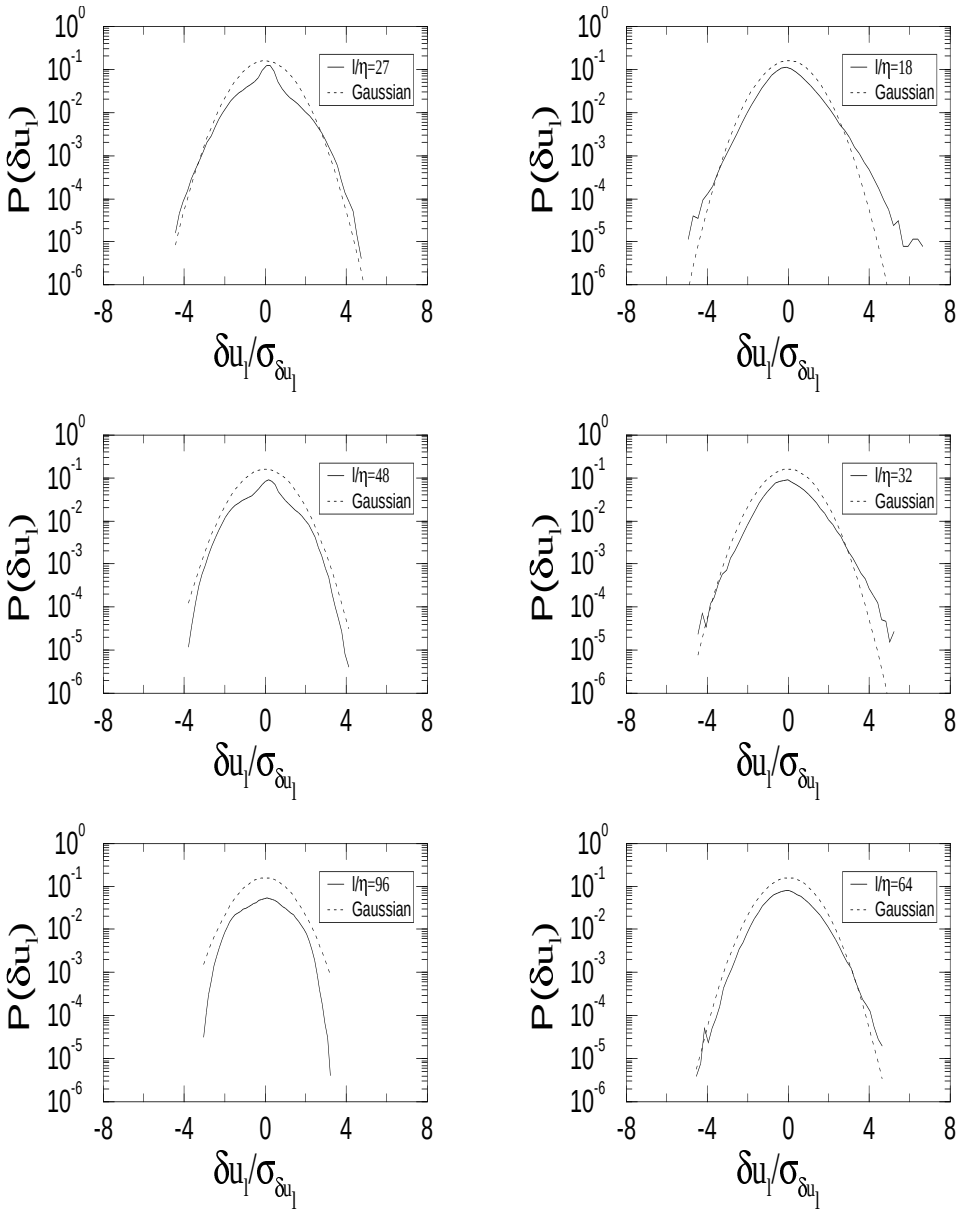

Figure 5.34: The probability distribution function for cylinder turbulence, for the lateral plane $Y/D = 0$ and for different ℓ/η, at downstream distances $X/D = 2$ and $X/D = 20$.

5.8 Jet and grid flows

In this section we present experimental results of two other very different flow configurations: jet and grid turbulence generated in a water channel. The two flow configurations are described in chapter 4, including the flow characteristics and the use of the sonic velocimeter SONTEK-3D probe. Due to the experimental limitations the time series of these experiments were short and the sampling frequency was only 25 Hz. Therefore, we are unable to examine the smallest scales and moreover the statistical limitations do not allow us to calculate Δ^* or the hierarchy $H^*(p,\ell)$, which needs very long time series.

5.8.1 Absolute energy transfer

As in the cylinder wake turbulence, the absolute energy transfer for jet and grid turbulence was calculated using the approximation (5.2). The results are presented in figures 5.35 and 5.36 for jet and grid turbulence respectively.

Figure 5.35: Local energy transfer σ_ℓ^* as a function of time for jet turbulence at the downstream distances $X/d = 7.5$ (top) and $X/d = 15$ (bottom) for three different scales $\ell_1 = 10\eta$, $\ell_2 = 20\eta$ and $\ell_3 = 30\eta$.

Figure 5.36: Local energy transfer σ_ℓ^* as a function of time for grid turbulence at the downstream distances $X/M = 5$ (top) and $X/M = 12$ (bottom) for three different scales $\ell_1 = 10\eta$, $\ell_2 = 20\eta$ and $\ell_3 = 30\eta$.

The figures illustrate the behavior of the local energy transfer σ_ℓ^* for different scales ℓ as a function of time for jet turbulence at the downstream distances ($X/d = 7.5, 15$) and for grid turbulence at the downstream distances ($X/M = 5, 12$). The figures demonstrate two different anomalies, the non-local dynamics related to the non-uniformity in scale of the energy transfer random field and the intermittency related to the largest but rarest events. The non-local dynamics at these locations is related to the flow being non-homogeneous.

5.8.2 Third-order structure function

Figures 5-37 and 5-38 show the ratio of $R = \langle \delta u_\ell^3 \rangle / \langle \mid \delta u_\ell \mid^3 \rangle$ as a function of non-dimensional scale ℓ/η at two downstream distances ($X/d = 7, 15$) for the jet and ($X/M = 5, 12$) for the grid. As mentioned in section 5.2 the ratio R depends on the separation distance ℓ. This indicates that the scaling properties of the two quantities $\langle \delta u_\ell^3 \rangle$ and $\langle \mid \delta u_\ell \mid^3 \rangle$ are not the same for non-homogeneous flows. However, even in homogeneous turbulence the proportionality between the two quantities is not always satisfied, as demonstrated by Herweijer (1995) in his investigations concerning homogeneous jet and grid turbulence.

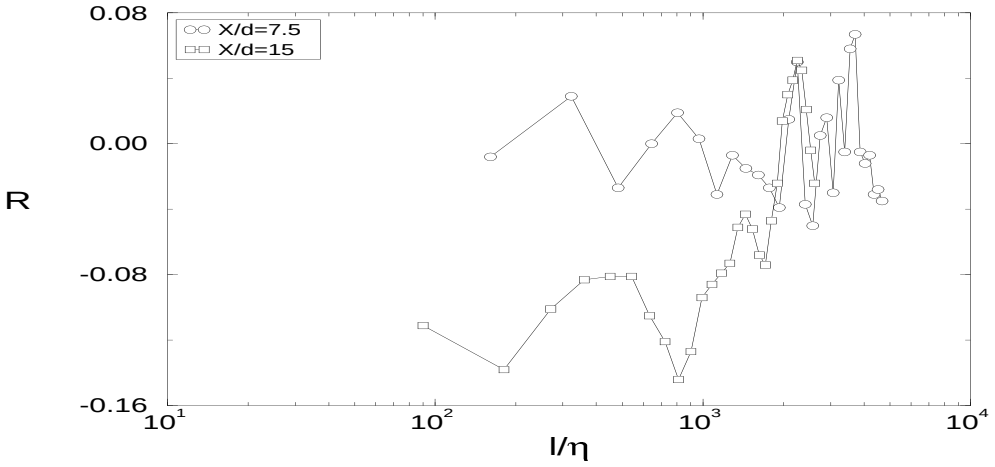

Figure 5.37: Ratio between $\langle \delta u_\ell^3 \rangle$ and $\langle \mid \delta u_\ell \mid^3 \rangle$ as a function of ℓ/η at the downstream distances $X/d = 7.5, 15$ from the jet nozzle.

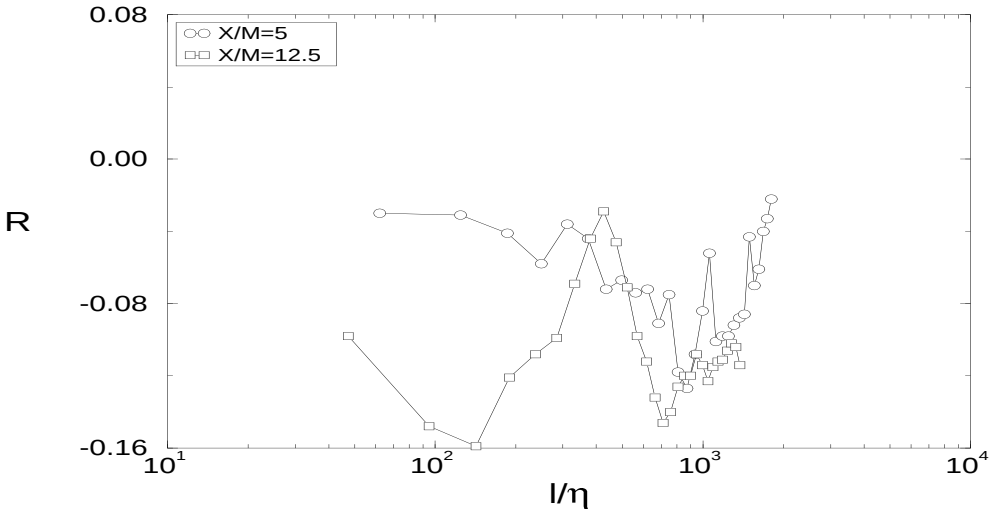

Figure 5.38: Ratio between $\langle \delta u_\ell^3 \rangle$ and $\langle \mid \delta u_\ell \mid^3 \rangle$ as a function of ℓ/η at the downstream distances $X/M = 5, 12.5$ from the grid.

5.8.3 Absolute scaling exponent ζ_3 and relative scaling exponent ζ_p/ζ_3

Figures 5-39 and 5-40 show the absolute scaling exponent ζ_3 for jet and grid turbulence as a function of non-dimensional scale ℓ/η, at different downstream distances along the symmetry axis. For jet turbulence, at short downstream distances near the source at $X/d = 7.5$, $X/d = 10$ and $X/d = 12.5$ there is a small zone where ζ_3 is constant, but the value of ζ_3 is different from 1, the value predicted by Kolmogorov (1941, 1962). Far away from the jet source ζ_3 shows a strong scale dependence on ℓ. For grid turbulence, ζ_3 is shown to depend on the separation distance ℓ at all downstream distances.

Figures 5-41 and 5-42 show the pair relative scaling exponents ζ_2/ζ_3, ζ_4/ζ_3 and ζ_6/ζ_3 as a function of downstream distance on the symmetry axis, for the jet and grid turbulence respectively. The values of the relative scaling exponents $\bar{\zeta}_p$ were calculated using the ESS technique described in chapter 3. It is clear that the relative scaling exponents ζ_p/ζ_3 do not have constant values either for a jet or grid turbulence, and these values depend on the downstream distance. The values of ζ_p/ζ_3 deviate from the Kolmogorov law K41, consistent with the experimental results of cylinder turbulence. This further demonstrates that ζ_p/ζ_3 is not constant in non-homogeneous flows.

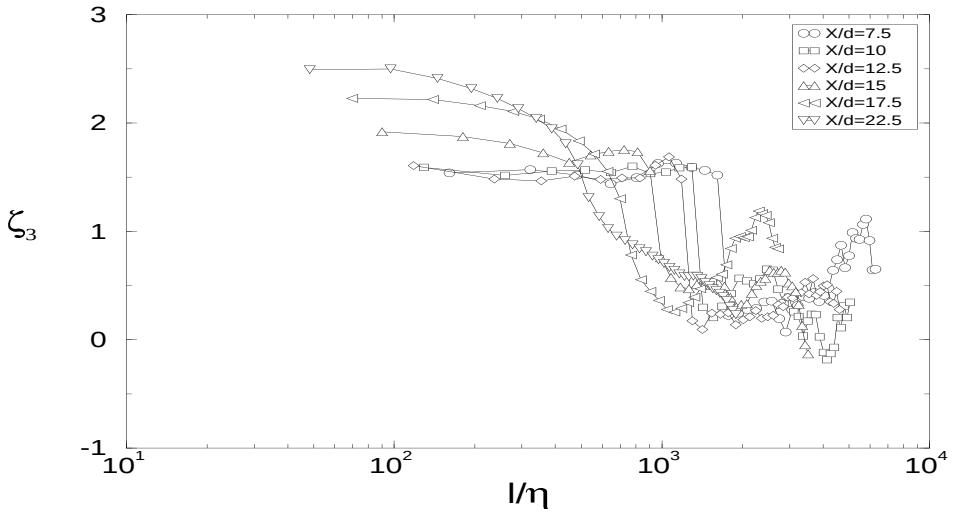

Figure 5.39: Third order absolute scaling exponent ζ_3 as a function of ℓ/η at different downstream distances X/d from the jet nozzle.

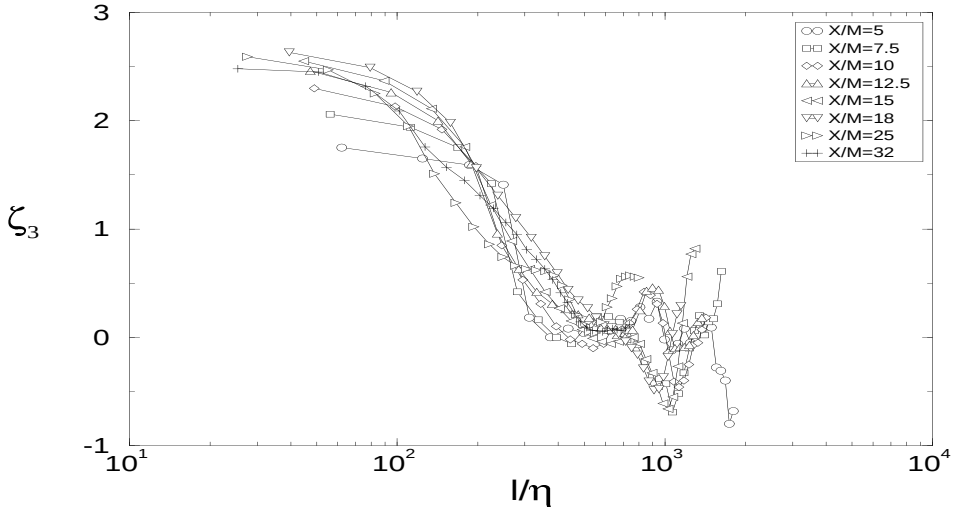

Figure 5.40: Third order absolute scaling exponent ζ_3 as a function of ℓ/η at different downstream distances X/M from the grid.

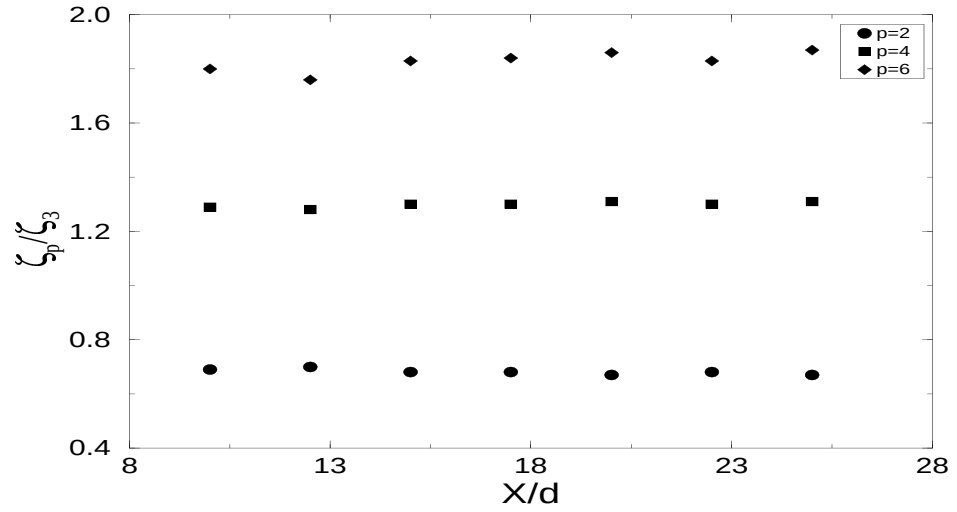

Figure 5.41: Relative scaling exponents ζ_p/ζ_3 for $p = 2, 4, 6$ at different downstream distances X/d from the jet nozzle.

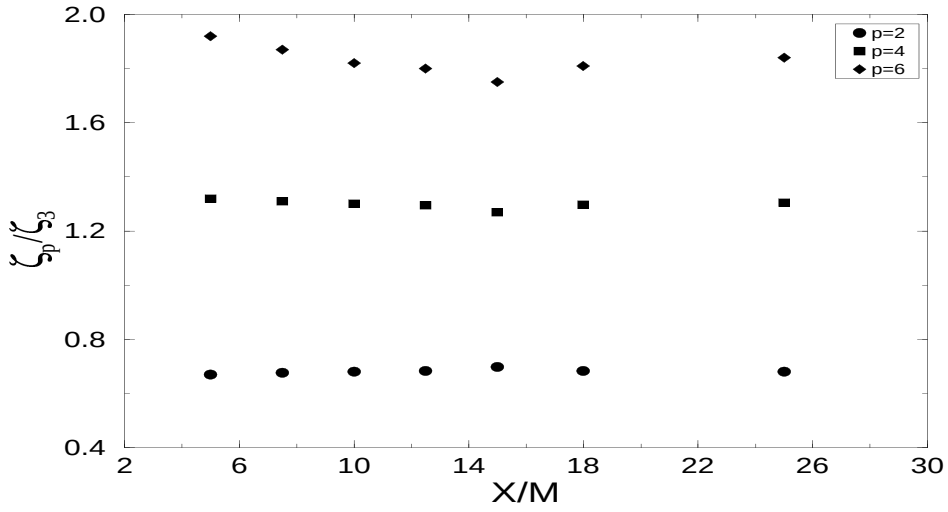

Figure 5.42: Relative scaling exponents ζ_p/ζ_3 for $p = 2, 4, 6$ at different downstream distances X/M from the grid.

5.9 Intermittency parameters μ and β

As for the wake turbulence, we have calculated the two intermittency parameter μ and β. Figures 5.43 and 5.44 show the behavior of μ as function of the downstream distance from jet nozzle and grid respectively. It can clearly be seen that μ depends on the location in the flow for both jet and grid turbulence. However, the two flows studied show different evolution of intermittency. Figures 5.45 and 5.46 illustrate the evolution of β as function of the downstream distance from jet nozzle and grid respectively. The intermittency parameter β has different evolutions for jet and grid, and these evolutions depend on the order p. Near the jet nozzle the flow is more intermittent, probably due to the distribution of the coherent structures near the jet nozzle. Far away from the jet nozzle β has higher values and is close to 0.9 at $X/d = 25$. Near the grid the value of β is close to 1, which indicate that the flow is practically homogeneous and non-intermittent. As the turbulence decays the flow becomes more intermittent, as shown in figure 5.46. At about $X/M = 15$ the wall boundary layers begin to affect the large-scale structures and the breaking of these large-scales structures provides a mechanism for a decrease of intermittency.

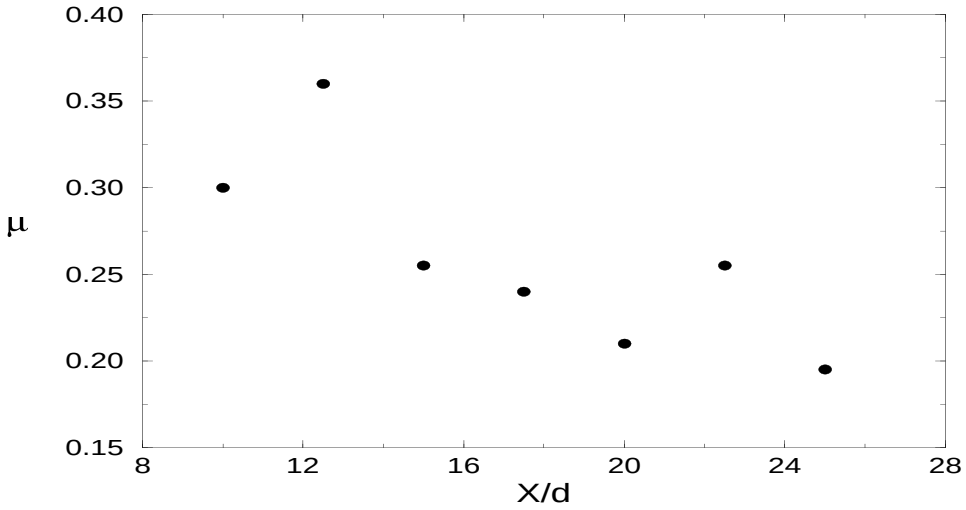

Figure 5.43: Variation of the intermittency parameter μ with the downstream distance X/d from the jet nozzle.

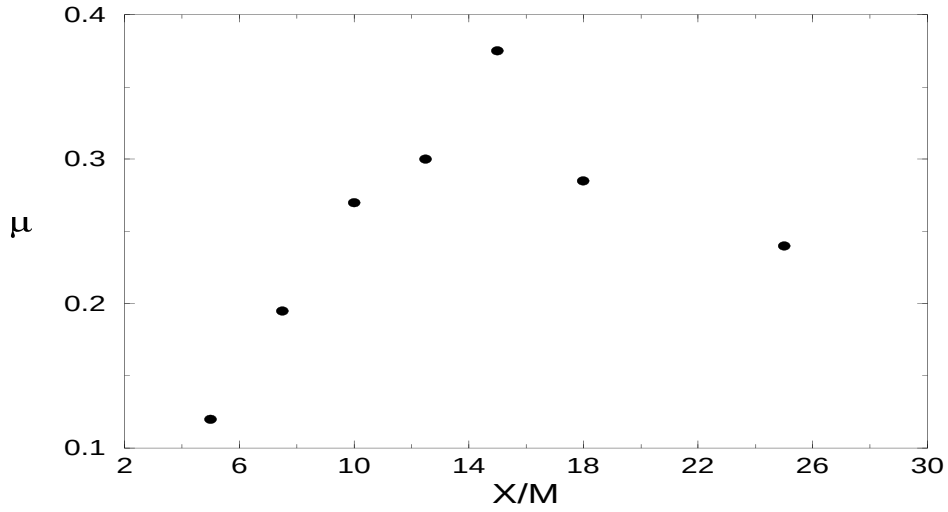

Figure 5.44: Variation of the intermittency parameter μ with the downstream distance X/d from the grid

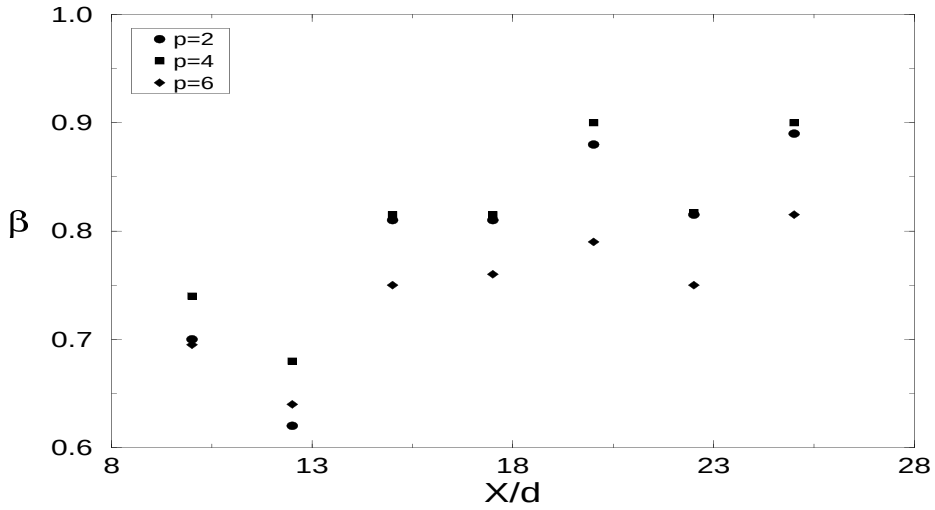

Figure 5.45: Variation of the intermittency parameter β with the downstream distance X/d from the jet nozzle.

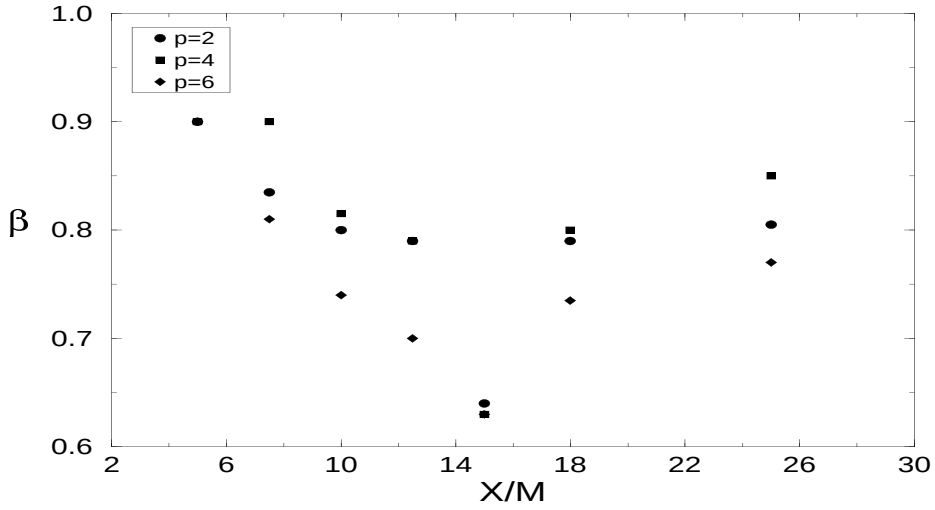

Figure 5.46: Variation of the intermittency parameter β with the downstream distance X/M from the grid